Version March 14, 2022
Preprint typeset using LaTeX style emulateapj v. 08/22/09

arXiv:1712.03197v1 [astro-ph.EP] 8 Dec 2017

MAJOR OUTBURST AND SPLITTING OF LONG-PERIOD COMET C/2015 ER_{61} (PAN-STARRS)

Zdenek Sekanina
Jet Propulsion Laboratory, California Institute of Technology, 4800 Oak Grove Drive, Pasadena, CA 91109, U.S.A.
Version March 14, 2022

ABSTRACT

In early April 2017, five weeks before passing through perihelion, the dust-poor comet C/2015 ER_{61} was observed to undergo a major outburst, during which its intrinsic brightness increased briefly by about 2 mag. Evidence is presented in this paper to suggest that the flare-up was in all likelihood a product of an event of nuclear fragmentation that gave birth to a companion nucleus, which was first detected more than nine weeks later, on June 11, and remained under observation for 19 days. The companion is found to have separated from the parent nucleus with a velocity of less than 1 m s^{-1}; subsequently it was subjected to a nongravitational deceleration of 14 units of 10^{-5} the Sun's gravitational acceleration. The companion's overall dimensions can from this value be estimated at less than one hundred meters across. Unlike the primary nucleus, the companion displayed considerable fluctuations in brightness on time scales spanning at least three orders of magnitude, from a fraction of one hour to weeks. The long temporal gap between the companion's birth and first detection appears to be a corollary of the brightness variability. Evidence from the light curve suggests that the companion became detectable only because of large amounts of debris that it started shedding as well as increased activity from areas newly exposed by progressive fragmentation, the same process that also resulted in the companion's impending disintegration by the end of June or in early July.

Subject headings: comets: individual (C/2015 ER_{61}) — methods: data analysis

1. INTRODUCTION

First spotted in several images taken under auspices of the Pan-STARRS Project with the 180-cm f/2.7 Ritchey-Chrétien reflector on Haleakalā, Maui, on March 14–15, 2015 (Gibson et al. 2015),[1] this object was of star-like appearance and classified as an asteroid 2015 ER_{61} by the *Minor Planet Center* (2015), even though it was almost 9 AU from the Sun and approaching it along a nearly-parabolic orbit with a perihelion distance comparable to 1 AU. The object was subsequently detected in several earlier Pan-STARRS images from January and February 2015 (Primak et al. 2016; Gibson et al. 2016). When signs of cometary activity were noticed by H. Sato in late December 2015 and confirmed by K. Sárneczky in January 2016, the object was re-classified as a long-period comet (Green 2016). However, an original barycentric reciprocal semimajor axis of $+0.001389 \pm 0.0000005$ AU^{-1} and the corresponding orbital period of $19\,320 \pm 10$ yr (Nakano 2017) demonstrate conclusively that the comet has not arrived from the Oort Cloud.

A typical dust-poor comet by its appearance (see Section 2.4), C/2015 ER_{61} was brightening steadily along its inbound orbit until a major outburst was reported in progress on April 4, 2017 (King 2017), the brightness having eventually risen to magnitude 6 (Green 2017a) before the flare-up began to subside a few days later.

Two months after this event, on June 13, a double nucleus was observed by E. Bryssinck (Green 2017b); the primary component, referred to hereafter as nucleus A, was accompanied by a very faint companion B, of apparent magnitude ∼16, located in the primary's coma some 0′.2 away in an essentially antisolar direction (Hambsch et al. 2017a; Masi & Schwartz 2017). Subsequently, the companion was identified in two June 11 images, in which it was still a bit fainter (Hambsch & Bryssinck 2017). The last of 52 astrometric observations of the companion come from June 30 (Hambsch et al. 2017b),[2] by which time it faded to magnitude 17. The orbital arc thus covers 19 days, long enough to warrant an in-depth investigation of the companion's motion.

Given the notoriety of temporal correlations between outbursts and nuclear fragmentation of many comets (e.g., Sekanina 1982, 2010; Boehnhardt 2004), the prime objective of this paper is the examination of a chance that the observed outburst and nuclear duplicity of C/2015 ER_{61} are, indeed, products of the *same event*. An important part of this task is the outburst's comprehensive analysis, focused in particular on the best possible determination of the time of its inception, a critical parameter for testing the significance of the correlation between the outburst and the nucleus' breakup.

2. LIGHT CURVE AND THE ONSET OF THE OUTBURST

To derive a dependable light curve of a comet is a difficult task, because the procedure requires that two contradictory conditions be satisfied simultaneously: (i) the temporal density of the data points be as high as possible and (ii) the data points be photometrically as homogeneous as possible. This second stipulation is equivalent to providing a *common magnitude scale* for all data sources (data source = observer + telescope used). An optimum solution inevitably demands a delicate balance between the two constraints.

For sets of magnitudes of C/2015 ER_{61}, the second condition could in practice be accommodated, to a limited degree, by applying constant corrections to the individual

Electronic address: Zdenek.Sekanina@jpl.nasa.gov
[1] See also *Minor Planet Circulars Supplement*, MPS 592555.
[2] All 52 available astrometric observations of the companion are listed in *Minor Planet Circulars* 105299–105300.

sources, which may conveniently be determined graphically by superposing transparencies with the light curves on top of one another until an optimum match has been achieved among them (Section 2.2).

2.1. *Light Curve from CCD Observations*

A fairly coherent light curve was constructed by combining the sets of total CCD magnitudes[3] reported by five Japanese observers. This combined dataset offers one major advantage: because of a very limited geographic distribution of the observers, they imaged the comet at practically the same time of the day, to within an hour or so of one another, so that the magnitudes they reported from the same dates refer to virtually coincident times and provide an opportunity to derive averaged systematic corrections between the observers' magnitude scales that are unaffected by the comet's intrinsic brightness variations on the time scales as short as ∼0.1 day.

Although three of the five observers began to record the magnitudes of C/2015 ER_{61} as early as February–April 2016, I examine their light curves only from the second half of November 2016 on, still nearly six months before perihelion, when the magnitude reports arrived in earnest after a gap of more than four months, after the comet emerged from a conjunction with the Sun. The examined dataset was terminated in the second half of June 2017, some six weeks after perihelion. During the more than seven months covered, the five CCD observers made a total of 54 determinations of the comet's brightness. Of primary interest was the period of three months, from early February 2017 to perihelion, which covers the reported outburst.

The five observers are listed in Table 1, which includes their abbreviations employed below, their locations and observatory codes, the telescopes used, the number of observations made, and the number of temporally coincident observations that are used below to derive the systematic magnitude corrections. Marked in the table is the reference observer, to whose magnitude scale the corrections for the other observers are referred.

The self-explanatory Table 2 presents a list of the temporally coincident observations by the five Japanese observers over a period of more than two months approximately centered on the comet's perihelion time. This information can readily be employed to compute the magnitude offsets between any two among the five observers, whose averaged values will become the adopted corrections. To start with, let for a pair of observers, X, Y, for which $\mathsf{X}=\{\mathsf{Ab},\mathsf{Ka},\mathsf{Oh},\mathsf{Se},\mathsf{Ta}\}$, $\mathsf{Y}=\{\mathsf{Ab},\mathsf{Ka},\mathsf{Oh},\mathsf{Se},\mathsf{Ta}\}$, and $\mathsf{X}\neq\mathsf{Y}$, the reported magnitudes at a given time be, respectively, $H(\mathsf{X})$ and $H(\mathsf{Y})$, and let their difference,

$$\Re(\mathsf{X},\mathsf{Y}) = H(\mathsf{X}) - H(\mathsf{Y}), \tag{1}$$

be referred to as an offset of the magnitude reported by observer Y from the magnitude reported simultaneously by observer X. If there is a third reporting observer, Z, one can always write Equation (1) as

$$\begin{aligned}\Re(\mathsf{X},\mathsf{Y}) &= \Re(\mathsf{X},\mathsf{Z}) - \Re(\mathsf{Y},\mathsf{Z}) \\ &= \Re(\mathsf{X},\mathsf{Z}) + \Re(\mathsf{Z},\mathsf{Y}).\end{aligned} \tag{2}$$

[3] These magnitudes, published by the *Minor Planet Center*, are marked T in order to distinguish them from the so-called nuclear magnitudes; see `http://www.minorplanetcenter.net/db_search`.

Table 1
Japanese Observers and Their CCD Magnitude Sets Used to Generate Light Curve of Comet C/2015 ER_{61}

Observer's name	Abbreviation	Location	Obs. Code	Telescope Used[a]	Magnitudes	
					Total	Coin.
Kadota, K.[b]	Ka	Ageo	349	25-cm f/5.0	17	6
Abe, H.	Ab	Yatsuka	367	26-cm f/6.0	9	1
Ohshima, Y.	Oh	Nagano	D81	30-cm f/4.6	9	5
Seki, T.	Se	Geisei	372	70-cm f/10.0[c]	5	3
Takahashi, T.	Ta	Kurihara	D95	25-cm f/4.2	14	7

Notes.
[a] All reflectors.
[b] Reference observer.
[c] With f/5.0 focal reducer.

The purpose of introducing a reference observer, R, is to formalize the system of corrections among a number of observers: all magnitudes are eventually referred to observer R by an equation of type (2). It is convenient to adopt a rule that R be always the first argument of $\Re$ [i.e., X in Equation (2)]. If so, the symbol for an offset of a magnitude reported by observer Z relative to a magnitude reported at the same time by the reference observer R can formally be simplified:

$$\Re(\mathsf{R},\mathsf{Z}) \equiv \Re(\mathsf{Z}), \tag{3}$$

so that an offset of magnitudes by two non-reference observers, Y and Z, can be expressed by

$$\Re(\mathsf{Y},\mathsf{Z}) = \Re(\mathsf{Z}) - \Re(\mathsf{Y}). \tag{4}$$

Before turning to Table 2, it is useful to recall that from magnitudes reported by n different observers for

Table 2
List of Temporally Coinciding Japanese CCD Observations[a] of Comet C/2015 ER_{61}

Time of Observation 2017 (UT)	Time from Perihelion (days)	Reported Magnitude, $H(\mathsf{Obs})$	Observer
Apr. 13.76	−26.19	7.9	Ohshima
13.78	−26.17	8.5	Takahashi
13.80	−26.15	7.8	Kadota
13.80	−26.15	7.5	Seki
Apr. 22.76	−17.19	7.1[b]	Ohshima
22.80	−17.15	8.5	Abe
May 1.77	−8.18	8.3	Ohshima
1.78	−8.17	9.0	Takahashi
May 3.76	−6.19	8.9	Takahashi
3.79	−6.16	8.6	Abe
May 18.73	+8.78	9.2	Takahashi
18.76	+8.81	8.8	Kadota
May 20.75	+10.80	9.3	Takahashi
20.77	+10.82	8.8	Kadota
May 28.74	+18.79	7.9[b]	Ohshima
28.74	+18.79	9.7	Takahashi
June 22.75	+43.80	10.6	Ohshima
22.76	+43.81	9.8	Kadota

Notes.
[a] Limited to times within two months from perihelion.
[b] Inconsistent with other entries; pair not used.

a given time one can derive N independent magnitude offsets, where

$$N = \tfrac{1}{2}n(n-1), \tag{5}$$

that is, one offset from magnitudes by two observers, three offsets from magnitudes by three observers, etc.

The magnitude offsets generated from the data in Table 2 can be divided into two groups: those including an observation by the reference observer Ka and those excluding it. There is a total of 11 offsets. Of these six include Ka: three from April 13 and one each from May 18, May 20, and June 22. Among these, three are Ta offsets, two Oh offsets, and one Se offset. Five offsets exclude Ka: three from April 13 and one each from May 1 and May 3. Among these, two relate Oh with Ta and one relates Ab with Ta, Oh with Se, and Se with Ta.

The N_{X} indidivual determinations of the offsets of the magnitude scale of each observer, X, relative to the reference observer are averaged in order to derive an effective correction, $\langle\Re(\mathsf{X})\rangle$,

$$\langle\Re(\mathsf{X})\rangle = \frac{1}{N_{\mathsf{X}}}\sum_{(\mathsf{X})}\Re(\mathsf{X}). \tag{6}$$

The offsets that do not include an observation by the reference observer have first to be converted to include Ka using Equation (4). Of the four non-reference observers in Table 1, it is noticed from Table 2 that offsets of magnitudes by observer Ab relative to the reference observer are unavailable. Offset $\Re$(Ab) should therefore be used as an independent variable in a search for a minimum sum of squares of residuals for all available offsets $\Re$(X) of the non-reference observers,

$$\sum_{(\mathsf{X})}\left[\Re(\mathsf{X})-\langle\Re(\mathsf{X})\rangle\right]^2 = \min. \tag{7}$$

The procedure is apparent from Table 3. Its upper part presents the six offsets (α) through (ζ) that include Ka, the lower part converts the remaining offsets into the four conditions (ν) through (π), with the condition (ξ) having a double weight because of the averaging of the conditions (η) and (θ) carried out for the sake of convenience. Altogether one has for each assumed $\Re$(Ab) four $\Re$(Oh) conditions, (α), (β), and twice (ξ); three $\Re$(Se) conditions, (γ), (o), and (π); and four $\Re$(Ta) conditions, (δ), (ϵ), (ζ), and (ν).

A practical approach to the problem consists in choosing a value of $\Re$(Ab); calculating $\Re$(Oh), $\Re$(Se), and $\Re$(Ta) from (ν) through (π) in Table 3; averaging these offsets, as shown by Equation (6), to obtain the corrections $\langle\Re(\mathsf{Oh})\rangle$, $\langle\Re(\mathsf{Se})\rangle$, and $\langle\Re(\mathsf{Ta})\rangle$, respectively; calculating the 11 residuals; summing up their squares according to Equation (7); and repeating these steps until a minimum is found on the curve of the squares of residuals. The respective $\Re$(Ab) equals the correction $\langle\Re(\mathsf{Ab})\rangle$ and determines the corrections for the observers Oh, Se, and Ta relative to Ka.

Application of this approach leads to the following effective corrections to convert the magnitude observations of the four observers to that of Kadota:

$$\begin{aligned}\langle\Re(\mathsf{Ab})\rangle &= -0.52,\\ \langle\Re(\mathsf{Oh})\rangle &= -0.31,\\ \langle\Re(\mathsf{Se})\rangle &= +0.24,\\ \langle\Re(\mathsf{Ta})\rangle &= -0.61,\end{aligned} \tag{8}$$

Table 3
CCD Magnitudes Offsets for Five Japanese Observers

OFFSETS INCLUDING Ka OBSERVATIONS		
Offsets $\Re$(Oh)		
Apr. 13:	$\Re(\mathsf{Oh}) = -0.1$	(α)
June 22:	$\Re(\mathsf{Oh}) = -0.8$	(β)
Offset $\Re$(Se)		
Apr. 13:	$\Re(\mathsf{Se}) = +0.3$	(γ)
Offsets $\Re$(Ta)		
Apr. 13:	$\Re(\mathsf{Ta}) = -0.7$	(δ)
May 18:	$\Re(\mathsf{Ta}) = -0.4$	(ϵ)
May 20:	$\Re(\mathsf{Ta}) = -0.5$	(ζ)
OFFSETS EXCLUDING Ka OBSERVATIONS		
Offsets $\Re$(Oh,Ta)		
Apr. 13:	$\Re(\mathsf{Oh,Ta}) = \Re(\mathsf{Ta}) - \Re(\mathsf{Oh}) = -0.6$	(η)
May 1:	$\Re(\mathsf{Oh,Ta}) = \Re(\mathsf{Ta}) - \Re(\mathsf{Oh}) = -0.7$	(θ)
Average (η)+(θ):	$\Re(\mathsf{Oh,Ta}) = \Re(\mathsf{Ta}) - \Re(\mathsf{Oh}) = -0.65$	(ι)
Offset $\Re$(Oh,Se)		
Apr. 13:	$\Re(\mathsf{Oh,Se}) = \Re(\mathsf{Se}) - \Re(\mathsf{Oh}) = +0.4$	(κ)
Offset $\Re$(Se,Ta)		
Apr. 13:	$\Re(\mathsf{Se,Ta}) = \Re(\mathsf{Ta}) - \Re(\mathsf{Se}) = -1.0$	(λ)
Offset $\Re$(Ab,Ta)		
May 3:	$\Re(\mathsf{Ab,Ta}) = \Re(\mathsf{Ta}) - \Re(\mathsf{Ab}) = -0.3$	(μ)
Offset $\Re$(Ta)		
From (μ):	$\Re(\mathsf{Ta}) = \Re(\mathsf{Ab}) - 0.3$	(ν)
Offset $\Re$(Oh)		
From (ι)+(ν):	$\Re(\mathsf{Oh}) = \Re(\mathsf{Ab}) + 0.35$[a]	(ξ)
Offsets $\Re$(Se)		
From (κ)+(ξ):	$\Re(\mathsf{Se}) = \Re(\mathsf{Ab}) + 0.75$	(o)
From (λ)+(ν):	$\Re(\mathsf{Se}) = \Re(\mathsf{Ab}) + 0.7$	(π)

Note.
[a] Double weight.

with the sum of squares or residuals equal to 0.4390 mag^2 and a mean residual of ±0.21 mag. Referring the data points by Abe, Ohshima, Seki, and Takahashi to the magnitude scale of Kadota using the corrections in Equations (8), the resulting light curve is plotted in Figure 1.

This set of uniform observations suggests that the outburst began on 2017 March 28.6 UT (with an estimated uncertainty of ±1 day), the amplitude was 2.8 mag (with an estimated uncertainty of ±0.1 mag), and the peak brightness was attained on about 2017 April 6.6 UT, or fully 9 days after the event's onset.

2.2. *Light Curve from Visual Observations*

To construct a light curve based on visual observations, I consulted three independent database websites: the *International Comet Quarterly*[4], Crni Vrh Observatory's *COBS database*[5], and the Iberoamerican Astronomical

[4] See `http://www.icq.eps.harvard.edu/CometMags.html`.
[5] See `http://www.cobs.sl/analysis`.

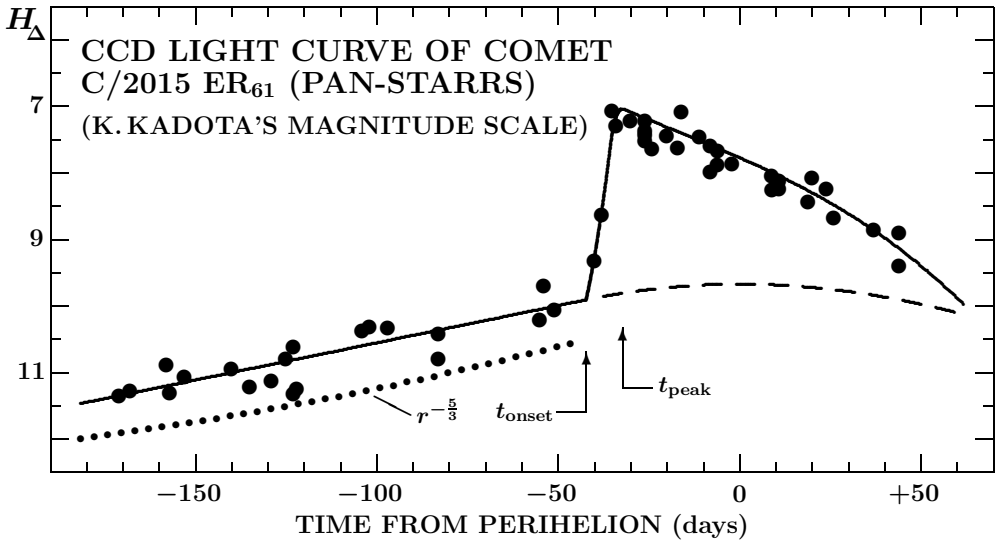


Figure 1. Light curve of comet C/2015 ER$_{61}$ based on the CCD observations by five Japanese observers (the so-called total magnitudes, as published in the *Minor Planet Center*'s database), normalized to Kadota's magnitude scale. The magnitude H_Δ is corrected for a geocentric distance using an inverse square power law, but not for a phase effect. The outburst is found to have commenced on 2017 March 28.6 UT or 42.3 days before perihelion, with an estimated uncertainty of ±1 day. It appears to have peaked near April 6.6 UT or 33.3 days before perihelion, with the same estimated uncertainty. The amplitude amounted to 2.8 mag, that is, the comet brightened by a factor of 13. The dashed curve is an extrapolation of the pre-outburst light curve assuming perihelion symmetry. The dotted curve, shifted vertically down by ∼0.5 mag for clarity, shows a shallow $r^{-5/3}$ variation with heliocentric distance r. Only three out of the 54 data points were rejected, all reported by the same observer who made the comet much too bright by 1 mag or more on, respectively, March 3, April 22, and May 28. The comet's integrated magnitude was brighter than Kadota's scale suggests; at peak light the comet was 1.2 AU from the Earth.

League's *Comet Observations* (LIADA) site[6], limiting the period of time to an interval from the beginning of January (130 days before perihelion) to May 9, 2017 (perihelion). From the three largely overlapping sources I collected a total of some 160 visual observations from the critical period, which were reported by 26 observers using 43 different instruments. For analysis I employed only the datasets that included at least a few observations covering periods of time longer than several days. It turned out that this condition was not satisfied by 16 observers using 19 instruments. For the remaining sets by 14 observers using 24 instruments I examined the light curve with the aim to derive the magnitude corrections to bring the data to a common photometric scale; I chose the binocular observations by J. J. González as a reference set after I found that his magnitudes obtained with the 10×50 binoculars and the 25×100 binoculars provided a consistent set of data over a period of more than two months. I found that no constant correction factors could be derived for four remaining observers (each with one instrument) to link their magnitudes with the rest of the data. I was thus left with 112 brightness estimates by 11 observers with 20 instruments to employ in constructing the visual light curve displayed in Figure 2; the corrections to González's scale were determined by a graphical method, as described at the start of Section 2.

To illustrate the effect of introducing the magnitude-source corrections to the data, I compare in Figure 3 a partial visual light curve before (left) and after (right) the appropriate corrections have been applied to the magnitudes reported by six observers (P. Camilleri, 40.6-cm reflector, *corr* = −0.40 mag; M. Goiato, 22-cm reflector, −1.25 mag; C. Hergenrother, 5-cm binoculars, +0.05 mag;

[6] See `http://rastreadoresdecometas.wordpress.com`.

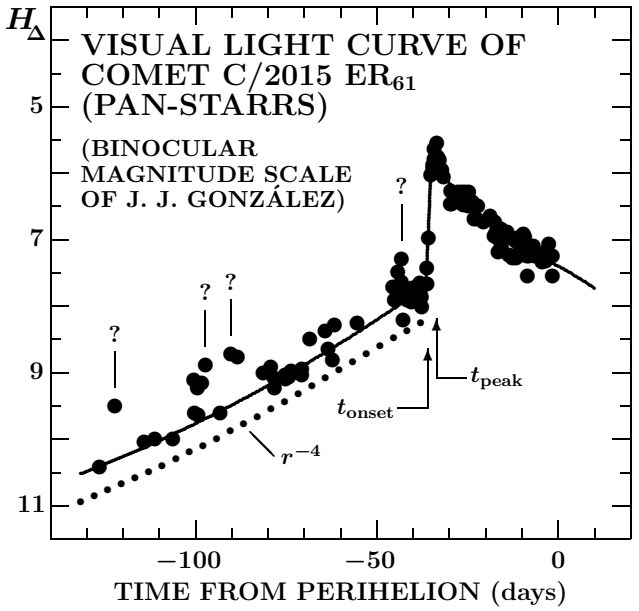


Figure 2. Preperihelion light curve of comet C/2015 ER$_{61}$ based on 112 visual magnitude estimates, reported by 11 observers (with 20 instruments) and normalized to the scale of J. J. González's binocular observations. The outburst is found to have begun most probably on 2017 April 3.9 ± 0.1 UT or 36.0 days before perihelion and to have peaked only 2.6 days later, 33.4 days before perihelion (with an uncertainty of about ±1 day). Compared with the results in Figure 1, the outburst is now determined to have started more than 6 days later, the time between the onset and the peak is about 6.5 days shorter, and the amplitude amounts to 2.1 mag, 0.7 mag shallower. There appear to be up to four minor flare-ups between the beginning of 2017 and the end of March (indicated by the question marks), although these are likely to be due to errors of observation (see the text). The pre-outburst brightness varies with heliocentric distance in this case more steeply, as r^{-4}. For additional information, consult the caption to Figure 1.

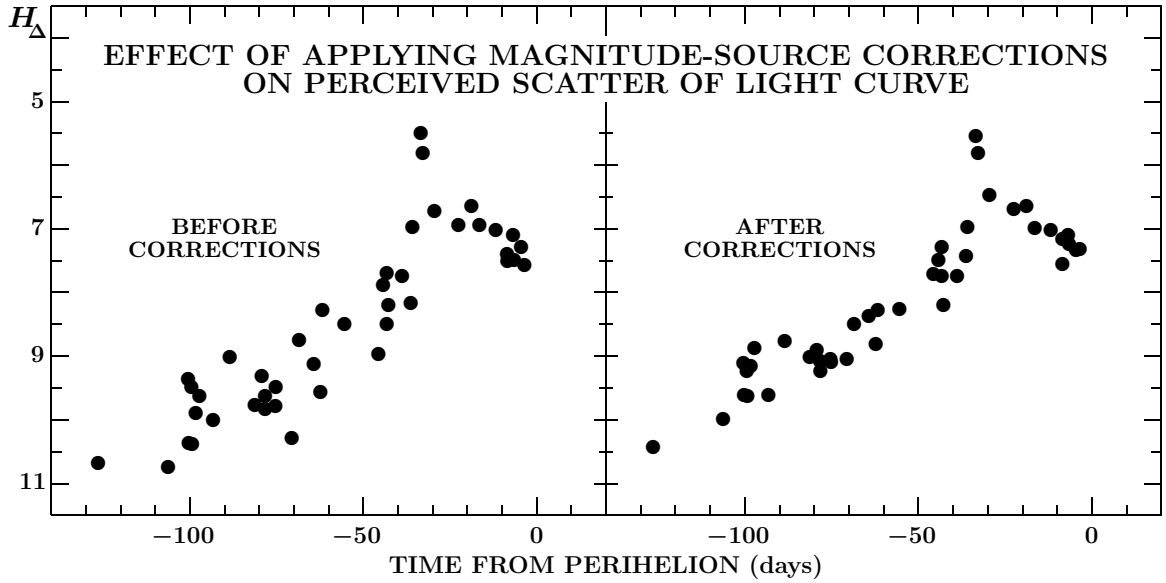


Figure 3. Comparison of a light curve before (left) and after (right) applying magnitude-source corrections to the data reported by six observers: P. Camilleri, 40.6-cm reflector; M. Goiato, 22-cm reflector; J. J. González, 5-cm and 10-cm binoculars; C. Hergenrother, 5-cm binoculars; T. Lehmann, 10.6-cm refractor; and C. Wyatt, 25-cm reflector. Note the dramatically reduced scatter on the right. See the text for the correction factors used and captions to Figures 1 and 2 for additional information.

T. Lehmann, 10.6-cm refractor, −0.25 mag; and C. Wyatt, 25-cm reflector, −0.75 mag; in addition to González with 5-cm and 10-cm binoculars, no correction). The figure, an example with arbitrarily selected observers, demonstrates that the uncorrected light curve exhibits much greater scatter than the corrected curve. Fitting the pre-outburst segment of the curve with a straight line yields a mean residual of ±0.48 mag before correction but only ±0.30 mag after correction, a drop by a factor of 1.6.

Having now a measure of the light curve's scatter, it is possible to address an issue of the nature of the four apparent minor flare-ups on the pre-outburst light curve in Figure 2. The marked highest points lie above the fit to the base data by, respectively from the left to the right, 0.83 mag, 0.82 mag, 0.79 mag, and 0.68 mag, that is, between 2.2σ and 2.8σ and therefore still within the standard 3σ limit of observational error. While the comet's intrinsic variation cannot be entirely ruled out, it is unlikely. This conclusion is particularly significant for the last of the four peaks, which occurs on March 27.7 UT (or 43.2 days before perihelion), within 24 hr of the onset time derived from the CCD-based light curve.

The visual light curve differs from the CCD-based light curve. M. Mattiazzo reported the comet to be of magnitude 8.3 on April 3.80 UT, of equal brightness as two days earlier, while 9 hr later, on April 4.17 UT González estimated it at 7.4, 0.7 mag brighter (when accounting for the scale difference between the two observers), implying a brightening rate of 1.9 mag day^{-1}. Thus, the event could not start before April 3.8 UT, over 6 days later than suggested by the CCD magnitudes. From the constraints I estimate that the outburst began on April 3.9 ± 0.1 UT, more than 6 days later than suggested by the CCD magnitudes, and peaked on April 6.5 UT (with an estimated uncertainty of ±1 day), at a time nearly identical with that derived from the CCD-based light curve; the amplitude now amounted to 2.1 mag (with an estimated uncertainty of ±0.1 mag), 0.7 mag less than in Figure 1.

2.3. *Light Curve from Nuclear Magnitudes*

I consider the disparity between the two results for the outburst disconcerting enough to warrant further investigation. In a previous paper dealing with the outbursts of comet 168P/Hergenrother I suggested (Sekanina 2010) that, when carefully analyzed and interpreted, the so-called nuclear CCD magnitudes — referring in fact to the brightness of an inner coma, commonly reported by the observers with astrometric observations of comets to the *Minor Planet Center*, and identified in the *Minor Planet Circulars* by a symbol N to distinguish them from the total CCD magnitudes (discussed in Section 2.1) — can be employed to great advantage as a diagnostic tool for determining the onset of cometary outbursts. This is so because outbursts are known to start with the sudden appearance and steep brightening of an unresolved plume of material called euphemistically in the comet jargon a "stellar nucleus" and described by a nuclear magnitude.

The results of application of this approach to comet C/2015 ER_{61} were short of expectations in terms of the gathered amount of data, but still led to a resolution of the disparity between the two light curves. Focused on the 70-day period from late February to the end of April 2017 (from 80 to 10 days before perihelion), I searched the *Minor Planet Center*'s C/2015 ER_{61} database (cf. footnote 3 in Section 2.1) for observatories that reported nuclear magnitudes both before and after the outburst. I was disappointed to find only three:

(1) Code J22, Tacande Observatory, La Palma, Islas Canarias, Spain (K. Hills, 50-cm f/2.9 astrograph, 10 obs.);

(2) Code C10, Observatoire de Maisoncelles, near Saint-Martin-du-Boschet, Seine-et-Marne, France (J.-F. Soulier, 30-cm f/3.8 reflector, 7 obs.); and

(3) Code A77, Observatoire Chante-Perdrix, Dauban, Alpes-de-Haute-Provence, France (J. Nicolas, J.-F. Soulier et al., 20-cm f/4 Schmidt-Cassegrain, 40-cm f/3 reflector, 41-cm f/3.3 reflector, 7 obs.).

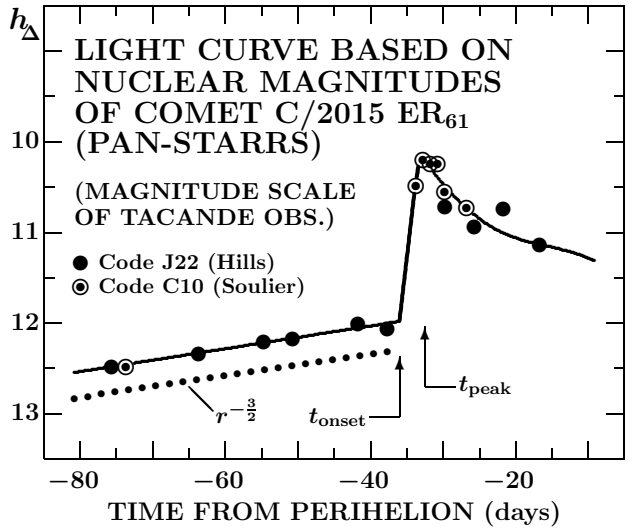


Figure 4. Preperihelion light curve of comet C/2015 ER$_{61}$ based on 17 CCD nuclear magnitudes, as published in the *Minor Planet Center*'s database. The plotted magnitudes, h_Δ, were corrected for a geocentric distance using an inverse square power law (but not for a phase effect) and normalized to the magnitude scale of the Tacande Observatory (code J22). Note that the two Tacande Observatory data points on March 29 and April 2 (41.7 and 37.7 days before perihelion) are not elevated, thus supporting the onset time of the outburst as derived from the visual light curve (Figure 2), but not from the CCD-based light curve (Figure 1). The onset time derived from the visual light curve is in fact employed in fitting the nuclear magnitudes. The pre-outburst variations with heliocentric distance follow a law of $r^{-3/2}$, much more flat than the visual light curve but comparable to the CCD-based curve.

Comparing the three datasets, it was noticed at once that the nuclear magnitudes reported by code A77 referred to a much smaller fraction of the nuclear condensation than the other data, being 2 mag fainter than the C10 data and 2.5 mag fainter than the J22 data in late February and by up to nearly 2 mag fainter than either of the two sets around the time of the outburst. Consequently, it was prudent to exclude the A77 data from the set.[7]

Unlike the A77 data, the nuclear magnitudes from the codes J22 and C10 could readily be combined into one set after a minor scale correction has been applied. The resulting light curve, plotted in Figure 4, provides for the outburst a scenario that in terms of the onset time accommodates the result from the visual light curve but not from the CCD-based light curve: two critical observations, on March 29.2 UT and April 2.2 UT, show that the brightness of the nuclear condensation was not yet elevated. The onset time derived from the visual light curve is employed in Figure 4 to show that the two light curves are compatible. The nuclear magnitudes suggest that the outburst peaked on about April 7.5 UT (with an estimated uncertainty of ±1 day), in fair agreement with the results from the visual and CCD-based light curves. The amplitude is now a little lower, 1.8 ± 0.1 mag, perhaps an effect of exclusion of the contributions from the outside of the nuclear condensation.

[7] An additional problem with the code A77 data is the use of up to three different telescopes; because of the overly succinct format in which the *Minor Planet Center* requires observers to present their observations, it is unclear which of the three telescopes was used for which of the reported nuclear-magnitude observations, thus introducing potentially some undesirable instrumental effects.

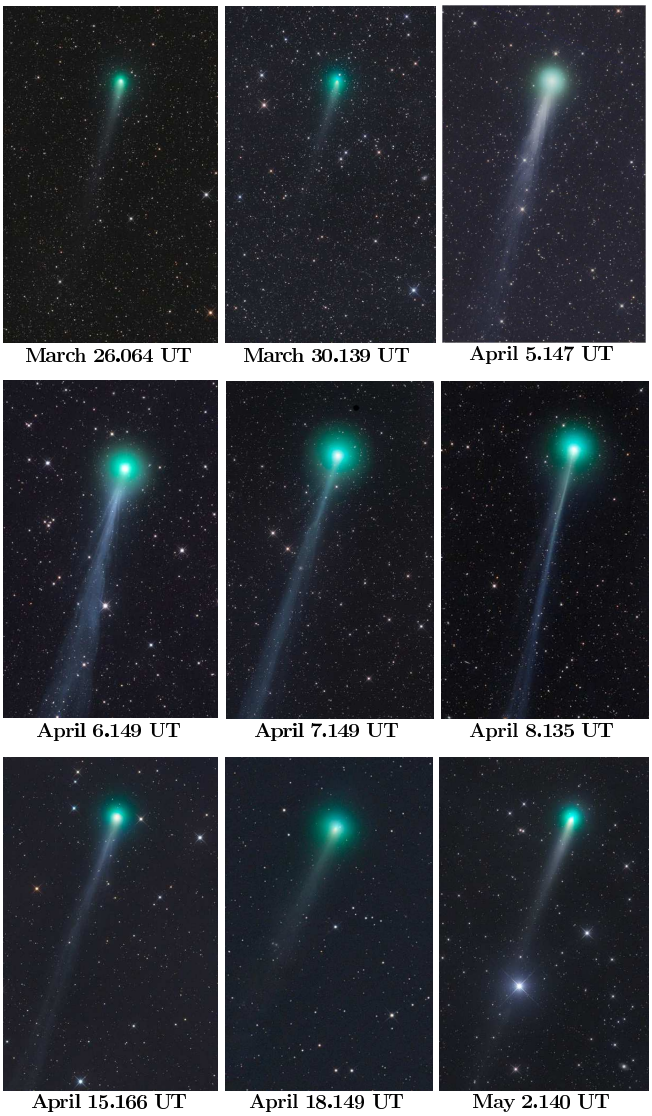


Figure 5. LRGB images of comet C/2015 ER$_{61}$ taken by G. Rhemann of Austria between March 26 and May 2, 2017 with a 30-cm f/3.6 astrograph at Farm Tivoli, Namibia. The total (L+R+G+B) exposure times were, chronologically: 24, 39, 27, 27, 27, 27, 39, 20, and 35 minutes. Each field extends about 80′ along the diagonal. An approximate orientation has the north to the right and the east up. Qualitatively, the comet appears to be the brightest on the images of April 5–8, fading gradually afterwards. While the brightness perception is, to a degree, affected by the uneven exposure times, the comet looks distinctly fainter on the two images from late March, consistent with the onset time of the outburst in early April, as derived from the visual light curve and the nuclear magnitudes. (Image credit: G. Rhemann, Astro Systeme Austria.)

2.4. *Evidence from Large-Scale Imaging and Dust-Content Data*

As an additional, though rather qualitative, test of the outburst timing, Figure 5 displays nine images of the comet taken by G. Rhemann with a 30-cm f/3.6 astrograph at Farm Tivoli in Namibia between March 26 and May 2, 2017.[8] Somewhat uneven exposure times notwithstanding, the comet clearly appears to be much fainter in the first two images, from late March, than

[8] See `http://www.astrostudio.at/2_Bright Comets.php`.

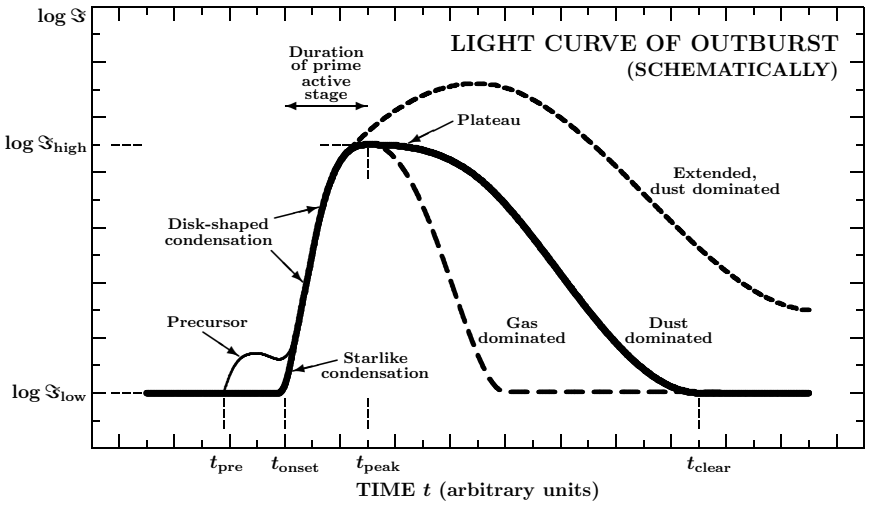


Figure 6. Schematic representation of the light curve of outbursts. The brightness, $\Im$, is plotted on a logarithmic scale against time, t. Four categories of events are depicted: a generic dust-dominated outburst (solid curve), an extended dust-dominated outburst (short-dashed curve), a gas-dominated outburst (long-dashed curve), and a precursor eruption. The first three types of events begin at the onset time, $t_{\rm onset}$, when the brightness is $\Im_{\rm low}$, while the inception of a precursor eruption and a composite explosion takes place at time $t_{\rm pre}$. A giant explosion can be described by scaling the curve for the generic dust-dominated outburst. The precipitous rise in brightness, which includes the appearance of a star-like condensation, is terminated at time $t_{\rm peak}$, the end of the prime active phase, when $\Im$ reaches a maximum, $\Im_{\rm high}$. The brightness then begins to subside slowly along a plateau in a dust-dominated outburst, until it drops to $\Im_{\rm low}$ at time $t_{\rm clear}$. By this time, all material ejected during the outburst has left the volume of the coma. For an extended dust-dominated outburst, the coma continues to brighten after $t_{\rm peak}$ and its brightness remains elevated after $t_{\rm clear}$ because of, e.g., an increasing cross-sectional area of continuously fragmenting dust particles. In a gas-dominated outburst, the brightness subsides much more rapidly, reaching $\Im_{\rm low}$ long before $t_{\rm clear}$. The symbol $\Im$ refers normally to the comet's total brightness, but it could also apply to the brightness of the nuclear condensation.

in the following ones, suggesting that the outburst did not begin before March 30.2 UT, in conformity with the results derived from the visual light curve and nuclear magnitudes, but contrary to what was found from the CCD-based light curve. I see no need for any correction to the onset time as presented in Section 2.2.

Finally, a set of measurements of $Af\rho$, a proxy of the dust-production rate (A'Hearn et al. 1995), is also consistent with the same outburst timing. For an aperture of 10 000 km, a Spanish website[9] lists the $Af\rho$ values measured by numerous observers to average ∼600 cm over a four-month period ending March 31, 2017, but to amount to ∼2000 cm on three nights between April 6 and 13, equivalent crudely to the dust-production rates of 0.6 and 2×10^6 g/s, respectively. Comparison with some preliminary water-production rates suggests that the dust-to-gas production rate ratio for this comet is low, in line with the object's bulb-like (or onion-like; from the German word *Zwiebelgewächs*; e.g., Bobrovnikoff 1927, 1928) appearance (Section 1).

3. TYPES AND PARAMETERS OF COMETARY OUTBURSTS

In my previous paper on the subject (Sekanina 2010), I defined an outburst of a comet as its "sudden, prominent, and unexpected brightening, caused by an abrupt, short-term injection of massive amounts of material" from the nucleus into the atmosphere. In Section 2.3 I already mention that, observationally, outbursts begin with the sudden appearance and precipitous brightening of a "stellar nucleus." This feature develops into a rapidly expanding disk with a progressively decreasing surface brightness, until it eventually disappears.

[9] See `http://www.astrosurf.com/cometas-obs` .

Outbursts appear to be activated by gases liberated from a reservoir of a highly volatile material stored in the nucleus that becomes heated up and/or pressurized. The products observed in the optical wavelegths are (i) the escaping gases that radiate in that spectral range and (ii) solid material, or dust, that, dragged from the nucleus by the outflowing gases, scatters sunlight. Depending on which of the two components prevails, one distinguishes between *dust-dominated* and *gas-dominated* outbursts. They have some common features but differ in other respects, as depicted schematically in Figure 6. An important common feature is an *active phase*: the activity of the outburst source on the nucleus begins at the time of onset and terminates, in a basic timeline, at the time of peak light, i.e., the duration of the active phase is defined by the interval between the onset and the peak. On the other hand, the differences between the two types of outburst are exemplified by a *plateau* — characterizing *only* the dust-dominated outbursts — which extends from the point of peak light on for a limited period of time and along which the comet's brightness subsides only gradually. By contrast, the peak on the light curve of the gas-dominated outbursts is followed by a steep decline in brightness, whose rate almost equals the rate of the initial brightening. This is so because the brightness variations in the gas-dominated outbursts are determined by the fairly short dissociation and ionization lifetimes of the radiating molecules in the coma (usually a day or so near 1 AU from the Sun), coupled with relatively high gas velocities (∼1 km s^{-1}). On the other hand, because of lower velocities of solid particles (in fact, dramatically lower velocities for heavier grains), the residence times of dust in the coma are substantially longer than the residence times of radiating molecules, hence a post-peak plateau in the dust-dominated outbursts.

The timeline of an outburst can be more complicated; if it is preceded by one or more *precursor eruptions*, the event becomes a *composite explosion*. Also, dust particles might fragment in the atmosphere, expanding their total cross-sectional area and increasing the comet's brightness over a longer period of time; such a scenario is referred to as an *extended dust-dominated* outburst.

The sources of outbursts have typically a fairly limited extent on the scale of nuclear dimensions, so most outbursts can be classified as local or, at the most, regional episodes. Exceptionally, a major part of the nucleus may get involved, so such events are of a global extent on the scale of nuclear dimensions, with potentially severe implications for the comet's future evolution; they are referred to here as *giant explosions*. The total mass released from a comet in a giant explosion amounts to or exceeds 10^{13} grams, orders of magnitude more than in a typical outburst.

Comparing the light curves of the various types of outburst, Figure 6 has been adapted from Sekanina (2010). The presented scenario assumes that a background level of the comet's activity before, during, and after the event is constant. The description of the active phase requires four basic data points: time $t_{\rm onset}$ and magnitude $\mathcal{H}_{\rm onset}$ for the onset and time $t_{\rm peak}$ and magnitude $\mathcal{H}_{\rm peak}$ for the peak light of the outburst, with an unknown time of peak injection rate preceding $t_{\rm peak}$. It is convenient to reckon time from the perihelion passage, t_π, by introducing

$$\tau_{\rm point} = t_{\rm point} - t_\pi, \qquad {\rm point} = {\rm onset, peak}. \tag{9}$$

The time interval, interpreted as the duration of an active phase of the outburst, is a nominal parameter referred to as a *rise time*, $\Delta\tau$,

$$\Delta\tau = \tau_{\rm peak} - \tau_{\rm onset} = t_{\rm peak} - t_{\rm onset} > 0. \tag{10}$$

The other nominal parameter is an *amplitude*, $\mathcal{A}$, of the outburst, defined as

$$\mathcal{A} = -(\mathcal{H}_{\rm peak} - \mathcal{H}_{\rm onset}) > 0. \tag{11}$$

Since $\Delta\tau$ typically equals a few days, the geocentric distance barely changes over $\Delta\tau$, unless the comet is rather close to the Earth. Accordingly, in a general case it hardly makes any difference whether the magnitudes are apparent or corrected for the geocentric distance. In the latter instance $\mathcal{H}_{\rm onset} = (H_\Delta)_{\rm onset}$ and $\mathcal{H}_{\rm peak} = (H_\Delta)_{\rm peak}$ for a CCD-based (Figure 1) and visual (Figure 2) light curve, but $\mathcal{H}_{\rm onset} = (h_\Delta)_{\rm onset}$ and $\mathcal{H}_{\rm peak} = (h_\Delta)_{\rm peak}$ for a light curve based on the nuclear magnitudes (Figure 4). In the following, I consistently use the magnitudes corrected for the geocentric distance.

The two nominal parameters can be combined into an *average flare-up rate*, Λ_0, to describe the rate of increase in brightness in the early stage of an outburst,

$$\Lambda_0 = \frac{\mathcal{A}}{\Delta\tau}. \tag{12}$$

The rate of fading after the outburst has peaked distinguishes dust-dominated outbursts from gas-dominated outbursts, as already remarked above.

The problem with this definition of the flare-up rate is the magnitude as a logarithmic quantity. In particular, if the comet is very faint at the onset of the outburst, its amplitude may become exceedingly high even if the amount of material released during the event is not very large. For this reason, it is more meaningful to express the brightness in flux units, namely,

$$\mathcal{F}_{\rm point} = f_0\, 10^{-0.4\mathcal{H}_{\rm point}}, \qquad {\rm point} = {\rm onset, peak}, \tag{13}$$

which allows one to define a *flux rise* between the onset and peak brightness of the outburst by

$$\Delta\mathcal{F} = \mathcal{F}_{\rm peak} - \mathcal{F}_{\rm onset} = f_0\, 10^{-0.4\mathcal{H}_{\rm peak}} \left(1 - 10^{-0.4\mathcal{A}}\right), \tag{14}$$

where $\mathcal{F}_{\rm point}$ is technically an illuminance from the comet (at 1 AU from the Earth) when the units of the constant f_0 are, e.g., lux = lumen m^{-2} or phot = lumen cm^{-2}. However, $\mathcal{F}_{\rm point}$ could instead represent the comet's irradiance, that is, a radiant flux received by a surface per unit area when f_0 is in units such as, e.g., W m^{-2} or photons cm^{-2} s^{-1}. If the magnitudes $\mathcal{H}_{\rm onset}$, $\mathcal{H}_{\rm peak}$ in Equations (13) and (14) refer to the top of the Earth's atmosphere (i.e., an unattenuated flux) and are visual magnitudes (i.e., a flux integrated over the Johnson-Cousins standard V passband, with a central wavelength of 0.55 μm), then $f_0 = 0.88 \times 10^6$ photons cm^{-2} s^{-1}; if, instead, the data are red magnitudes (i.e., an unattenuated flux integrated over the Johnson-Cousins standard R passband with a central wavelength of 0.64 μm), then $f_0 = 1.07 \times 10^6$ photons cm^{-2} s^{-1} (Bessell 1979).[10] Since both visual and CCD-based magnitudes are dealt with in this paper (the transmission curves of the CCD sensors differing from the standard passbands), I will employ below $f_0 = 10^6$ photons cm^{-2} s^{-1} as a rounded-off orientation value.

When the amplitude $\mathcal{A}$ is very large, the limiting value of the flux rise,

$$\lim_{\mathcal{A}\to\infty} \Delta\mathcal{F} = \Delta\mathcal{F}_\infty = f_0 10^{-0.4\mathcal{H}_{\rm peak}}, \tag{15}$$

depends only on the magnitude of the outburst peak. According to Equation (14), $0.9\Delta\mathcal{F}_\infty < \Delta\mathcal{F} < \Delta\mathcal{F}_\infty$ when $\mathcal{A} > 2\frac{1}{2}$ mag and $0.99\Delta\mathcal{F}_\infty < \Delta\mathcal{F} < \Delta\mathcal{F}_\infty$ when $\mathcal{A} > 5$ mag. This argument justifies the approximate determination of a flux rise for some outbursts and all giant explosions, for which the magnitude at the onset (and therefore the amplitude) is unavailable (e.g., when the comet is discovered during an outburst, such as 17P in 1892) but for which there exist grounds to believe that the comet brightened substantially during the event. In addition, this exercise suggests that by itself the amplitude is not a critical outburst parameter.

Equation (14) replaces (11) as a measure of the increase in brightness caused by the outburst. Similarly, the rate of brightening Λ_0 from Equation (12) is replaced with an *average rate of flux rise*,

$$\Lambda = \left\langle \frac{\partial\mathcal{F}}{\partial t} \right\rangle = \frac{\Delta\mathcal{F}}{\Delta\tau}, \tag{16}$$

where $\Delta\mathcal{F}$ comes from Equation (14) and $\Delta\tau$ from Equation (10); if the rate Λ is expressed in photons cm^{-2} s^{-2}, $\Delta\tau$ must be in seconds rather than days. Note that unlike $\Delta\mathcal{F}$, Λ cannot be determined (not even approximately) when for some reason there is no information on the outburst inception.

[10] See also `http://www.cfa.harvard.edu/~dfabricant/huchra/ay145/mags.html`.

If it should be desirable to normalize the flux-rise rate from Equation (16) to the comet's irradiance at the time of onset of the outburst, one can introduce an *average relative flux-rise rate*, λ,

$$\lambda = \frac{1}{\mathcal{F}_{\rm onset}} \left\langle \frac{\partial \mathcal{F}}{\partial t} \right\rangle = \frac{10^{0.4\mathcal{A}}-1}{\Delta\tau}, \qquad (17)$$

which, as expected, depends on both $\mathcal{A}$ and $\Delta\tau$; its dimension is $\rm day^{-1}$ or $\rm s^{-1}$. The new parameters $\Delta\mathcal{F}$, Λ, and λ are now ready to be compared to the nominal parameters $\mathcal{A}$ and Λ_0.

4. COMPARISON OF OUTBURSTS IN C/2015 ER_{61} AND OTHER COMETS

The nominal as well as newly introduced parameters are next employed to compare the outburst experienced by C/2015 ER_{61} with those that other, selected comets were subjected to, including the giant explosions that 17P/Holmes and 1P/Halley were observed to undergo; to investigate the range and distribution of the parametric values; and to illustrate the major differences between the nominal and flux-based parameters.

The results are summarized in Table 4, which is mostly self-explanatory. The data type in column 2 refers to the segment of the light curve that affects the outburst parameters, not necessarily to the whole curve: vis stands for visual observations, CCD for such (usually unfiltered) observations; comb for combined visual and photographic or CCD observations; and nucl for (CCD) nuclear magnitudes. As already noted, all employed observations were always first corrected, to the extent possible, for personal and instrumental effects, normalized to a common magnitude scale, and corrected to 1 AU from the Earth before a light curve was plotted, analyzed, and interpreted. The uncertainties in the normalized brightness data determine the errors of the parameters in the table, which generally range from a fraction of 1 day to a couple of days in $\Delta\tau$; 0.1 mag to a few tenths of magnitude in $\mathcal{A}$; the relative errors of $\Delta\mathcal{F}$, Λ, and λ are typically on the order of a few percent to a few tens of percent.

To cover a wide range of objects and explosive events, I compare C/2015 ER_{61} with objects subjected to both dust-dominated and gas-dominated events, including a variety of ordinary outbursts (both at the same apparition and at different apparitions for periodic comets) and all giant explosions that I am aware of; one of them is interpreted in two different ways, both as a single event and a composite explosion that consists of a precursor burst and a main eruption.

It is noted that the nominal parameters of ordinary outbursts and giant explosions overlap and thus are not diagnostic for discriminating between the two categories; in particular, a giant explosion is not identified by an enormous amplitude. On the other hand, two of the newly introduced parameters, the flux rise, $\Delta\mathcal{F}$, and the average flux-rise rate, Λ, separate the two categories of explosions quite distinctly. The first of them largely reflects the normalized magnitude at peak brightness, $\mathcal{H}_{\rm peak}$, so that when experiencing a giant explosion, the comet is intrinsically much brighter than when it is subjected to an outburst. The second condition is more subtle: when in a giant explosion, the comet brightens at a faster average pace than in an outburst.

Of the listed comets, the two successive 1973 outbursts of 41P were closest to the giant explosions in terms of $\mathcal{H}_{\rm peak}$; however, they were typical gas-dominated events, with the mass of dust released by 41P orders of magnitude lower than the amounts lost by 17P or 1P.

The superiority of the parameters $\Delta\mathcal{F}$ and Λ over the nominal ones, $\mathcal{A}$ and Λ_0, is also apparent from comparison of the four outbursts of comet C/2001 A2 (Sekanina et al. 2002). While the amplitude suggests that Event I was by far the most prominent among the four, the values of $\Delta\mathcal{F}$ show that, together with Event IV, Event I was in fact the least powerful and that the strongest one (by a factor of nearly 4 relative to Event I) was Event III, which may have incorporated precursors. Also in line with its respectable magnitude, this event accompanied the separation from the primary nucleus B of three companion nuclei, fully one half of the total of six detected.

Quite exceptional was the outburst of comet 73P in 1995, which related to a fragmentation of the parent nucleus resulting in the birth of the principal fragment C and a persistent companion fragment B. The rise time of 36 days encompassing the perihelion time, represents a record in Table 4. The event probably consisted of a number of successive flare-ups that gradually built the amplitude up to 5 mag. The post-peak evolution of the light curve was also peculiar. It first dropped at a moderate rate, only to develop into a second outburst (not tabulated here) of a much smaller amplitude, but of considerable plateau that extended over some 100 days.

Of a similar amplitude as the extended explosion of 73P was an October 1959 outburst of 29P/Schwassmann-Wachmann, an object that is famous for its propensity to flaring up. This event's timeline was described in great detail by Beyer (1962), who monitored the comet for three months by both measuring increasing coma dimensions and providing a visual light curve.[11] I extrapolate the measured coma-expansion rate to determine the time of outburst onset to ± 0.2 day. I estimate the normalized magnitude at onset at $\mathcal{H}_{\rm onset} = 12 \pm 0.5$ (equivalent to apparent magnitude 15.5) from the following information on the comet: (i) its nondetection by Beyer with a 26-cm refractor on September 27 and 30; (ii) its nondetection on patrol plates at the Sonneberg Observatory taken on September 30 (Beyer 1962); (iii) its photographic detection by Roemer (1959) with a 102-cm reflector on September 25; and (iv) its apparent magnitude at the quiescent phase averages about 16 (e.g., Trigo-Rodríguez et al. 2010). Compared to the 1995 event of 73P, the rise time is now one order of magnitude shorter, although the two events are alike in displaying an extremely long post-peak plateau.

Contrary to these two instances and the giant explosions, most cometary outbursts — including, among others, those of C/2015 ER_{61}, 41P, and C/2001 A2 — appear to be fairly short-lived, at least in terms of the total brightness, the light curve exhibiting a sharp peak rather than a plateau, that is, no signature of dust dominance. At first sight, this fact may look peculiar considering that the "stellar nucleus," appearing in the early phase of an outburst (Section 2.3), consists of a cloud of expand-

[11] This outburst was one of the most prominent on record (peak apparent visual magnitude of 10.7); competitive events reported in extensive recent investigations (e.g., Trigo-Rodríguez et al. 2010; Hosek et al. 2013; Miles et al. 2016) are very rare.

Table 4
Comparison of Outburst of C/2015 ER_{61} with Outbursts and Giant Explosions of Other Comets[a]

Comet	Data Type	Time from Perihelion (days) at Onset, τ_{onset}	Time from Perihelion (days) at Peak, τ_{peak}	Normalized Magnitude (mag) at Onset, $\mathcal{H}_{onset}$	Normalized Magnitude (mag) at Peak, $\mathcal{H}_{peak}$	Rise Time, $\Delta\tau$ (days)	Ampli-tude, $\mathcal{A}$ (mag)	Average Flare-Up Rate, Λ_0 (mag/day)	Flux Rise, $\Delta\mathcal{F}$ (units)[b]	Flux-Rise Rate Λ (units)[c]	Flux-Rise Rate λ (day^{-1})
Outbursts											
C/2015 ER_{61} (Pan-STARRS)											
C/2015 ER_{61} (Preferred sol.)[d]	vis	−36.0	−33.4	7.7	5.6	2.6	2.1	0.81	49	2.2	2.3
C/2015 ER_{61} (Inferior sol.)[e]	CCD	−42.3	−33.3	9.9	7.1	9.0	2.8	0.31	13	0.17	1.4
29P/Schwassmann-Wachmann											
29P (October 1959 event)[f]	vis	+871.8	+875.8	12	7.2	4.0	4.8	1.2	13	0.38	21
41P/Tuttle-Giacobini-Kresák											
41P (May 1973 event)	vis	−5	−2	13.5	4.5	3	9	3.0	160	6.1	1300
41P (July 1973 event)	vis	+35.6	+37.6	14	5	2.0	9	4.5	100	5.8	2000
73P/Schwassmann-Wachmann											
73P (major 1995 event)[g]	vis	−16	+20	10.2	5.2	36	5.0	0.14	82	0.26	2.8
73P-B (2006 event B-I)	CCD	−66.2	−61.5	13.6	9.9	4.7	3.7	0.79	1.1	0.026	6.2
73P-G (2006 event G-II)	CCD	−62.4	−57.4	17.2	14.1	5.0	3.1	0.62	0.022	0.0005	3.3
168P/Hergenrother[h]											
168P (2012 event I)	nucl	−30.4	−28.7	16.6	14.9	1.7	1.7	1.0	0.009	0.0006	2.2
168P (2012 event II)	nucl	−9.3	−5	15.4	13.0	4.3	2.4	0.56	0.056	0.0015	1.9
168P (2012 event III)	nucl	−0.2	+1	13.1	12.6	1.2:	0.5	0.42	0.034	0.003	0.5
C/2001 A2 (LINEAR)[i]											
C/2001 A2 (Event I)	vis	−57.0	−54.0	12.1	6.7	3.0	5.4	1.8	21	0.80	48
C/2001 A2 (Event II)	vis	−14.0	−10.5	6.4	5.3	3.5	1.1	0.31	48	1.6	0.50
C/2001 A2 (Event III)	vis	+11.5	+19.5	6.3	4.9	8.0	1.4	0.18	79	1.1	0.33
C/2001 A2 (Event IV)	vis	+48.0	+50.5	7.9	6.4	2.5	1.5	0.60	21	0.95	1.2
C/1999 S4 (LINEAR)											
C/1999 S4 (cataclysmic)[j]	vis	−6.8	−2.0	8.9	7.5	4.8	1.4	0.29	7.2	0.17	0.55
C/1996 Q1 (Tabur)											
C/1996 Q1 (cataclysmic)[j,k]	vis	−21	−19	7.2	6.2	2	1.0	0.5	20	1.2	0.76
Giant Explosions											
17P/Holmes											
17P (2007 event)[l]	comb	+172.2	+174.4	15.2	1.4	2.2	13.8	6.3	2750	145	15×10^4
17P (2007 event)[m] prec.	CCD	+172.14	+172.74	15.2	8.9	0.60	6.3	10.5	2.8	0.53	550
17P (2007 event)[m] main	comb	+172.20	+174.40	(15.2)	1.4	2.20	13.8	6.3	2750	145	15×10^4
17P (1892 event)[n]	vis	+144	+150	....	3.3	6	....	....	500:	9:	.....
17P (1893 event)[o]	vis	+216.0	+218	6.6	3.6	2	3.0	1.5	340	20	7.4
1P/Halley											
1P (1836 event)[p]	vis	+67.8	+70	4	0.3	2.2	3.7	1.7	7300	400	13

Notes.

[a] Unless stated otherwise, onset and peak data taken from Table 20 of Sekanina (2012), which is upgrade to Table 2 of Sekanina (2008a).

[b] Unit is 10^2photons/cm^2/s.

[c] Unit is 10^{-2}photons/cm^2/s^2.

[d] Derived from visual light curve.

[e] Derived from CCD-based light curve.

[f] Based on Beyer's (1962) observations.

[g] Parent comet; onset and peak data from Table 1 of Sekanina (2005a).

[h] Onset and peak data taken from Table 6 and Figure 2 of Sekanina (2010).

[i] Onset and peak data taken from Table 1 and Figure 1 of Sekanina et al. (2002).

[j] Terminal outburst, signaling impending complete disintegration of comet.

[k] Onset and peak data read from Figure 3 of Sekanina & Kracht (20116).

[l] Most recent giant explosion; onset and peak data taken from Table 3 of Sekanina (2009); interpreted as a single event.

[m] Same data as in l interpreted as a composite explosion, consisting of precursor and main burst.

[n] Comet discovered during this giant explosion; time of onset unknown, but extrapolated from observations of expanding halo.

[o] Second, slightly less powerful giant explosion at discovery apparition.

[p] Historically first known observation of giant explosion; onset and peak data are upgrade to Table 2 of Sekanina (2008b).

ing dust. The explanation has long been known: a close monitoring of a relatively modest outburst of 12P/Pons-Brooks on January 1, 1884 by Müller (1884a, 1884b) and independently by Vogel (1884) led both observers to conclude that while the coma brightness was dominated by three bands (of C_2), a continuous spectrum prevailed in the nuclear condensation and its outskirts. Hence, unless the amount of dust in the ejecta is overwhelming, its contribution to total light of the comet drops with time too rapidly to exhibit a plateau.

A special place among cometary explosions has the category of *terminal outbursts*, represented in Table 4 by comets C/1996 Q1 (Tabur) and C/1999 S4 (LINEAR). Unlike other outbursts, this type of flaring up is of cataclysmic nature, as it signals an imminent, complete disintegration of the comet in the course of several days to, at most, a few weeks following the outburst. Both tabulated events have a fairly modest amplitude, less than 1.5 mag. C/1996 Q1 was genetically related to C/1988 A1 (Liller) and C/2015 F3 (SWAN), making up a group of long-period comets with nearly identical orbits; of these, C/1988 A1 was the main mass, while C/1996 Q1 and C/2015 F3 were its companions. The group's history was recently investigated by Sekanina & Kracht (2016), where the reader can find the light curve of C/1996 Q1 from which the onset and peak data were read.

On the other hand, C/1999 S4 is not known to be the member of a comet group (or a pair), although it was suggested by Sekanina (2000) that this object could have been a trailing fragment of a more massive comet moving in a nearly identical orbit, whose arrival to perihelion, perhaps many centuries earlier, was missed.

The very low values of $\Delta\mathcal{F}$ and Λ for comet 168P are a product of, in part, the use of the nuclear (rather than total) magnitudes and, in part, the intrinsic faintness of the object. In fact, according to the COBS database (cf. footnote 5 to Section 2.2), the comet's total visual magnitude at peak brightness was less than 2 mag (or a factor of $\sim$5) above the nuclear magnitude.

By comparison, the investigated comet's outburst[12] is on a par with the outbursts of C/2001 A2, which — as noted above — were associated with a release from the parent nucleus of several nuclear fragments. It is therefore plausible to anticipate a possible temporal correlation between the outburst and splitting of C/2015 ER_{61}, a major objective of this paper.

For a temporal correlation with the companion's separation, it is the timing of the outburst that is of interest. Since it is reasonable to assume that the companion was most likely to break off from the parent comet in the course of the active phase of the outburst, the statistically probable fragmentation time can in this scenario be equated with the midtime of the event's active period, $t_{\rm mid}$ (with a probable uncertainty of one half of the rise time), that is,

$$t_{\rm mid} - t_\pi = \left(\tau_{\rm onset} + \tfrac{1}{2}\Delta\tau\right) \pm \tfrac{1}{2}\Delta\tau. \qquad (18)$$

The preferred solution in Table 4 gives for C/2015 ER_{61} $t_{\rm mid} - t_\pi = -34.7 \pm 0.5$ days or $t_{\rm mid} =$ 2017 April 5.2 UT.

[12] That is, its preferred solution; the inferior solution is tabulated to show a high degree of disparity compared to the preferred solution in all parameters, especially an order-of-magnitude discrepancy in the flux-rise rate.

5. BIRTH AND MOTION OF COMPANION NUCLEUS

To describe the heliocentric motion of the companion, or fragment B, I refer it to the primary nucleus, or fragment A, by modeling the temporal variations in the offsets "companion minus primary", or B – A, of the astrometric positions measured in images obtained by the same observer (or a group of observers) in right ascension and declination. An inherent part of this exercise is an assumption that the companion and the primary had a common parent in the past and that they seperated from each other at some particular time. The scenario thus involves a process of fragmentation of the original single nucleus — the problem of a split comet.

5.1. *The Offsets* B – A

When the astrometric positions of both fragments are measured in the same image, the generation of the B – A offset is straightforward. However, especially in recent times the astrometric positions of an object are derived from a set of short exposures by stacking the best of them to increase the signal and suppress the noise. If the sets of optimum images for the primary and the companion are not identical, the effective times of their stacked images generally differ.

In this study the selected offset times are always identical with the imaging times of the companion. To generate a B – A offset for any of these times when the imaging times of the two fragments do not coincide, it is necessary to convert the astrometric position of the primary nucleus from a nearby time to the time of the companion's astrometric position by applying a correction for the primary's heliocentric motion between the two times, employing a (high-quality) set of orbital elements. To achieve a meaningful result, only a primary-nucleus' position at a time that differs from the time of the companion's position by less than a small fraction of a day should be used. If there are multiple choices for a given time of the companion's position, the statistically best offset is derived by averaging all the individual offsets based on the primary's positions at times within the given limit from the time of the companion's position.

To compute the offsets of the companion from the primary of C/2015 ER_{61}, the maximum allowed time difference to be incorporated in the B – A offsets was adopted to be $\pm$0.01 day. As the comet's geocentric motion in the period of June 11–30 averaged about $+100''\,{\rm hr}^{-1}$ in right ascension and $+33''\,{\rm hr}^{-1}$ in declination, a crude estimate for a maximum correction to the primary's positions amount to $\pm 24''$ in right ascension and $\pm 8''$ in declination. Most corrections were of course substantially smaller than these approximate upper limits.

5.2. *Fragmentation Model*

Of the 52 astrometric observations of the companion (cf. Section 1 and footnote 2), three could not be used to derive the B – A offsets because of the unavailability of the astrometric positions for the primary. The 49 remaining offsets in right ascension and declination were derived as explained above from the two fragments' astrometric positions secured by six groups of observers listed in Table 5. The appearance of the comet's nuclear region on one of the images taken at San Pedro de Atacama, Chile, on June 19 is reproduced in Figure 7.

Table 5
Sources of Astrometric Observations of Nuclear Fragments of C/2015 ER_{61} for Generating B – A Offsets

Obs. Code	Observatory	Telescope Employed	Time Covered 2017 (UT)	Number of Offsets	Observer(s)
G39	Remote Observatory Atacama Desert, San Pedro de Atacama, Chile	40-cm f/6.8 astrograph	June 11.4–30.4	31	Hambsch, F.-J., et al.
926	Tenagra Observatories, Tenagra III, Nogales, Ariz., U.S.A.	41-cm f/3.75 astrograph	June 17.4–21.4	6	Masi, G., Schwartz, M.
G40	Slooh Canary Islands Observatory, Mt. Teide, Tenerife, I.C., Spain	43-cm f/6.8 Corr. Dall-Kirkham	June 16.2–20.2	4	Lütkenhöner, B.
Q62	iTelescope South–Siding Spring Obs., Coonabarabran, N.S.W., Australia	51-cm f/4.5 Ritchey-Chrétien	June 19.8	4	Bryssinck, E.
C10	Observatoire Maisoncelles, Saint-Martin-du-Boschet, France	30-cm f/3.8 Newtonian reflector	June 19.1	2	Soulier, J.-F.
W96	CampoCatino Austral Observatory, San Pedro de Atacama, Chile	40-cm f/5.4 Ritchey-Chrétien	June 23.4	2	Maury, A., et al.

The 49 B – A offsets were fitted by a multiparameter model for split comets (Sekanina 1978, 1982). Applying an iterative least-squares differential-correction procedure, the model allows one to solve for up to five parametric constants: the time of fragmentation (i.e., separation of the two objects), $t_{\rm frg}$; the post-split differential nongravitational deceleration of the companion relative to the primary nucleus (driven by anisotropic outgassing from the two objects and assumed to vary inversely as the square of heliocentric distance), γ; and the velocity of separation, $V_{\rm sep}$, of the companion, consisting of the components in three cardinal directions of the right-handed RTN coordinate system: the radial (away from the Sun) $V_{\rm R}$; transverse $V_{\rm T}$; and normal $V_{\rm N}$. Since the nongravitational deceleration varies, in principle, as the cross-sectional area of the object and inversely as its mass (i.e., in the sum inversely as the object's size) and since γ is a difference between the companion and the (presumably larger and more massive) primary, the model should always yield $\gamma > 0$. In addition, experience with the previously investigated comets suggests that the separtion velocity $V_{\rm sep}$ is generally quite low, mostly lower than 1 m s^{-1}, and that for a given split comet solutions with $V_{\rm sep} > 1$ m s^{-1} should be viewed as inferior, suspect, and not physically meaningful compared to solutions for which $V_{\rm sep} < 1$ m s^{-1}.

The model allows one to solve for all, or any combination of fewer than, the five parameters. The length of the covered arc of the companion's trajectory and the accuracy of the offsets constrain the number of parameters that can be solved for. Solutions with a number of parameters greater than this limit usually fail to converge because they are highly correlated. This is particularly true for the pair of the fragmentation time and the radial component of the separation velocity and for the pair of the deceleration and the transverse component of the velocity. On the other hand, one should always solve for at least two parameters. It is sometimes a fair approximation to adopt a zero value for $V_{\rm R}$, $V_{\rm T}$, and/or $V_{\rm N}$, even though the velocity's normal component is usually well determined. However, only under special circumstances makes it sense to assume $\gamma = 0$ (i.e., when the primary and companion are of comparable size and activity). No such approximation obviously applies to the fragmentation time. If the splitting of the nucleus is suspected to coincide with an outburst (or another event), its time could be adopted for $t_{\rm frg}$; this sort of a coincidence is exactly what I exploit below.

The various solutions are referred to below by a letter group in which F stands for the fragmentation time, D for the deceleration, and R, T, and N for the three separation velocity components. Thus, for example, Solution FD indicates that the only parameters solved for were $t_{\rm frg}$ and γ, while the other parameters were chosen (usually equated with zero except for $t_{\rm frg}$); Solution DRTN means that the deceleration and all three separation velocity components were solved for, while for the fragmentation time I adopted $t_{\rm frg} = t_{\rm mid}$ from Equation (18).

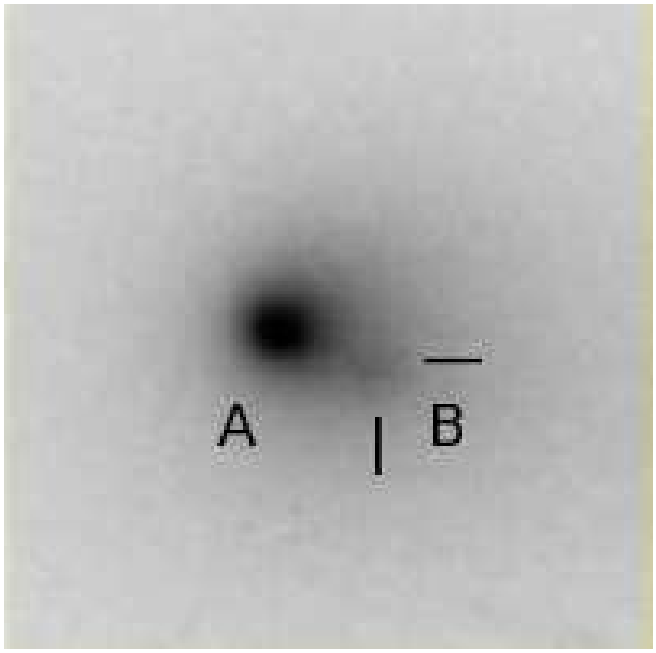


Figure 7. Image of the primary nucleus A and companion B of comet C/2015 ER_{61} taken by F.-J. Hambsch and E. Bryssinck with the 40-cm f/6.8 astrograph (+ CCD + R Bessell filter) of the Remote Observatory Atacama Desert, San Pedro de Atacama, Chile, on 2017 June 19.41 UT. The image is about 140″, or 152 000 km at the comet, along the diagonal. North is up, east to the left. (Image credit: E. Bryssinck, Brixiis Astronomical Observatory; `http://www.astronomie.be/erik.bryssinck/c2015er61.html`).

Table 6
Fragmentation Solutions[a] for the Companion of C/2015 ER_{61}

Solution	Fragmentation time, $t_{frg}-t_\pi$ (days)	Deceleration, γ (units)[b]	Velocity of Separation (m s^{-1})				Mean Residual (Sum of Squares of Residuals)	Comment
			V_{sep}	V_R	V_T	V_N		
DRN	*−34.7*	9.4 ± 1.5	0.72 ± 0.19	$+0.58 \pm 0.24$	.....	-0.42 ± 0.02	$\pm 0''.65$ (34.745)	
DRN^+	*−34.7*	5.8 ± 1.4	0.96 ± 0.18	$+0.72 \pm 0.24$	*+0.5*	-0.40 ± 0.02	$\pm 0''.65$ (34.802)	
DRN^-	*−34.7*	12.9 ± 1.5	0.79 ± 0.13	$+0.44 \pm 0.24$	*−0.5*	-0.43 ± 0.02	$\pm 0''.65$ (34.692)	
FDN	-50.4 ± 7.5	9.7 ± 1.1	0.38 ± 0.02	.....	.....	-0.38 ± 0.02	$\pm 0''.65$ (34.515)	$t_{frg} \neq t_{mid}$ by $>2\sigma$
DTN	*−34.7*	24.2 ± 4.5	2.15 ± 0.82	.....	-2.10 ± 0.84	-0.48 ± 0.04	$\pm 0''.65$ (34.552)	V_T correlated with γ
DRTN	*−34.7*	58 ± 52	7.0 ± 7.2	-1.4 ± 2.1	-6.9 ± 7.3	-0.64 ± 0.24	$\pm 0''.66$ (34.367)	γ,V_{sep} indeterminate
RTN	*−34.7*	.....	1.67 ± 0.19	$+0.96 \pm 0.18$	$+1.32 \pm 0.21$	-0.37 ± 0.03	$\pm 0''.66$ (34.904)	V_T absorbing γ effect
DN	*−34.7*	12.9 ± 0.1	0.40 ± 0.02	.....	.....	-0.40 ± 0.02	$\pm 0''.67$ (37.261)	systematic trends
FD	-27.1 ± 9.2	15.5 ± 3.9	.....	.....	.....	.....	$\pm 1''.51$ (187.90)	unacceptable trends

Notes.

[a] Parameters whose values were adopted rather than solved for are depicted by slanted font; if the adopted value (for γ, V_R, V_T, or V_N) was zero, the space is dotted.

[b] Units of 10^{-5} the Sun's gravitational acceleration, also referred to in the text as γ-units.

I searched for all 26 possible two- to five-parameter solutions of the fragmentation model when applying it to the companion of C/2015 ER_{61}; some, including the most successful, solutions are highlighted in Table 6. They are based on 42 consistent offsets with the residual in either coordinate not exceeding $\pm 1''.5$. The remaining seven offsets left higher residuals and were rejected. When not solved for, γ, V_R, V_T, and V_N were assigned a value of zero, unless specified otherwise in the table. As seen, in all but two tabulated solutions, t_{frg} was assumed to equal the midtime of the active phase of the detected outburst (Section 4). The findings of the model's application are summarized in the following.

5.3. *Results from Two-Parameter Solutions:* FD, FR, FT, FN, DR, DT, DN, RT, RN, *and* TN

None of these solutions is found to be satisfactory. The least unsatisfactory is Solution DN, listed in Table 6, which, however, leaves systematic residuals of up to about $0''.5$ in right ascension and a less prominent trend in declination, with a mean residual of $\pm 0''.67$. Solutions TN, RN, and RT, based on a dubious assumption of a zero deceleration, leave systematic trends of $\sim 1''$ or more in the distribution of residuals and a mean residual of, respectively, $\pm 0''.76$, $\pm 0''.80$, and $\pm 1''.28$. The other solutions with a zero assumed deceleration — FR, FT, and FN — fail to converge. The remaining three solutions — FD, DR, and DT — do not fare much better: the first two leave a very unsatisfactory mean residual of $\pm 1''.51$, whereas the last one, leaving a mean residual of $\pm 1''.11$, offers a physically meaningless negative nongravitational deceleration γ. Solutions DT, RT, and TN yield for the transverse component of the separation velocity undesirably high values in excess of 2 m s^{-1}.

5.4. *Results from Three-Parameter Solutions:* FDR, FDT, FDN, FRT, FRN, FTN, DRT, DRN, DTN, *and* RTN

This group includes the best solutions that dominate Table 6, DRN and FDN. In terms of fitting the measured positional offsets, they are equivalent, but the timing of the fragmentation event in Solution FDN is determined with a large mean error and deviates from the midtime of the active phase of the outburst by only $\sim 2\sigma$, suggesting a potential relationship between the two events. A third solution, DTN, also provides a satisfactory fit, but the transverse component of the separation velocity is rather poorly determined because of its high correlation with the deceleration. Four solutions — FDR, FRT, FRN, and FTN — fail to converge, while other two — FDT and DRT — yield a negative deceleration, again because of its high correlation with the transverse component of the separation velocity. The last solution — RTN — offers, as Table 6 illustrates. a separation velocity much higher than 1 m s^{-1}, as its transverse component is apparently forced to absorb the ignored effect of a deceleration.

5.5. *Results from Four-Parameter and Five-Parameter Solutions:* FDRT, FDRN, FDTN, FRTN, DRTN, *and* FDRTN

One common problem that these runs are consistently pointing to is too many unknowns. Fully five of the six solutions — FDRT, FDRN, FDTN, FRTN, and FDRTN — do not converge, while the sixth, presented in Table 6, shows both the deceleration and the separation velocity to be indeterminate, unquestionably again because of high correlations.

5.6. *Final Comments on Fragmentation of C/2015 ER_{61}. Companion's Longevity*

I find the temporal coincidence between the outburst and the fragmentation event rather compelling, as converging solutions that include the fragmentation time as an unknown variable have a tendency to bracket the time of outburst (see Table 6 for an example). I do not doubt that Solution DRN is the type of a solution that should provide the best results in this instance. Both Table 6 and Sections 5.3–5.5 suggest that it is counterproductive to solve simultaneously for the deceleration and transverse component of the separation velocity, as they always are very highly correlated, an option that Solution DRN avoids. It is also counterproductive to solve for more than three parameters, as the available database cannot support such elaborate solutions.

There is another observed property of the companion that has not as yet been examined — its lifetime against disintegration. This is the issue behind my presentation in Table 6 of two additional solutions: DRN^+, whose transverse component of the separation velocity is assumed to equal +0.5 m s^{-1}, and DRN^-, for which I adopt instead −0.5 m s^{-1}. The introduction of a change of 0.5 m s^{-1} is shown to force an opposite change of about 3.5 units of 10^{-5} the Sun's gravitational acceleration (called "γ-units" in the following) in the deceleration: a higher velocity requires a lower deceleration and vice versa. These parametric changes have only a negligible and physically irrelevant effect on the quality of fit, as is seen from the sum of squares of residuals in Table 6. Besides the deceleration, the other two components of the separation velocity are also affected, the radial moderately, the normal just slightly, but in either case by an amount that is comparable to their mean errors. The effects of an introduced V_T can be expressed numerically thus (all in the units used in Table 6):

$$\begin{aligned} \gamma &= 9.39 - 7.10\, V_T, \\ V_R &= +0.578 + 0.283\, V_T, \\ V_N &= -0.416 + 0.033\, V_T. \end{aligned} \tag{19}$$

From the second and third relations one gets

$$V_{sep} = \sqrt{1.081\, V_T^2 + 0.300\, V_T + 0.507}. \tag{20}$$

It follows that the separation velocity stays below 1 m s^{-1} as long as $-0.83\ \mathrm{m\ s^{-1}} < V_T < +0.55\ \mathrm{m\ s^{-1}}$; the deceleration is then confined to 5.5 γ-units $< \gamma <$ 15.3 γ-units. The separation velocity reaches a minimum of 0.70 m s^{-1} when $V_T = -0.14$ m s^{-1}; the deceleration then amounts to 10.4 γ-units. Thus, either of these conditions suggests that V_T is more likely to be negative and, accordingly, the deceleration probably exceeds 10 γ-units.

It turns out that there is an important relationship between the deceleration γ of a companion and its lifetime against disintegration or longevity. Based on their longevity, the companions are classified into three categories, each described by a distinct γ range (Sekanina 1982): persistent companions ($\gamma \le 7$ γ-units), short-lived companions (20 γ-units $\le \gamma \le$ 60 γ-units), and minor companions ($\gamma >$ 60 γ-units).

A measure of a companion's longevity is an *endurance*, E, defined as a minimum lifetime against disintegration weighted by outgassing (Sekanina 1982)

$$E = \int_{t_{frg}}^{t_{fin}} \frac{dt}{r^2} = 1.015\, [q(1+e)]^{-\frac{1}{2}} (u_{fin} - u_{frg}), \tag{21}$$

where t_{fin} is the time of last detection of the companion, u_{frg} and u_{fin} (in deg) the true anomalies at, respectively, t_{frg} and t_{fin}, r the heliocentric distance at time t, q the perihelion distance (in AU), and e the eccentricity of the orbit. The endurance E is then expressed in equivalent days at 1 AU from the Sun, or *e-days*. The demise of a companion is usually rather abrupt, characterized by a sudden loss of the condensation, dramatic fading, and rapid expansion and elongation of its apparent dimensions, all unquestionable signs of the object's disintegration into a cloud of small fragments and dust. As a rule, t_{fin} and u_{fin} are fairly well defined and so is E.

The available data suggest that the endurance correlates with the deceleration, following closely an empirical law (Sekanina 1982)

$$E = C\, \gamma^{-0.4}, \tag{22}$$

where C is a constant. There appear to be three classes of companions, which differ from one another by a degree of brittleness (or cohesion); most fragments (persistent, short-lived, and minor) of the split comets investigated in the 1980s were members of the class of average brittleness, for which $C = 200$ e-days. Among persistent companions there was, in addition, a class of low brittleness (sturdier material), for which C is about 4 times higher, while among short-lived and minor companions there also was a class of high brittleness (more fragile material) with C anout 2.3 times lower.

In broad terms, the results in Table 6 and analysis of conditions (19) and (20) suggest that the companion of C/2015 ER_{61} was subjected to a moderate deceleration that was close to an upper limit of the category of persistent companions but not high enough to qualify as a short-lived companion. However, because of a small database available in the 1980s, the limits of the categories were set rather arbitrarily. Since then there have been several instances of split comets with companions in the interim range between the persistent and short-lived companions (7 γ-units $< \gamma <$ 20 γ-units).[13]

It is fair to say that the companion of C/2015 ER_{61} was confined to a broad boundary region between the persistent and short-lived companions. The endurance E should unequivocally determine to which brittleness class the companion belongs. The value of E should also contribute to settling the issue of correlation among the parameters of the fragmentation model. Adopting for this companion $t_{frg} - t_\pi = -34.7$ days from Table 6 and $t_{fin} - t_\pi = +51.5$ days (that is, t_{fin} = 2017 June 30.4 UT; Table 7), I find that $u_{fin} - u_{frg} = 98°$ and $E = 69$ e-days.

One can readily rule out a chance of the companion belonging either to the class of low brittleness (requiring $\gamma \sim 460$ γ-units) or to the class of high brittleness (requiring $\gamma \sim 1.8$ γ-units). For a member of the class of average brittleness, E implies $\gamma = 14.3$ γ-units, well within the interval dictated by the condition $V_{sep} < 1$ m s^{-1} coupled with Equation (20). From Equations (19) it is now possible to derive the components of the separation velocity and thus obtain a solution that (i) fits the B − A offsets; (ii) complies with the condition that the fragmentation event closely correlated with the outburst; (iii) satisfies the condition of low separation velocity; and (iv) is consistent with the correlation between the deceleration

[13] A nice example is companion A of comet C/2001 A2, whose separation from the primary nucleus B correlated temporally with Outburst I (listed here in Table 4). The motion of this companion was affected by a deceleration $\gamma = 16.3 \pm 0.6$ γ-units (Sekanina et al. 2002) and its endurance was 63 e-days, in nearly perfect harmony with the law (22) for the class of companions of average brittleness. Other examples are the companion to comet C/2005 A1 (LINEAR) with $\gamma = 16.2 \pm 0.6$ γ-units (Sekanina 2005b); companions C (Solution III) and D_2 (Solution II) of comet 141P/Machholz with, respectively, $\gamma = 11.5 \pm 2.5$ and 15.9 ± 4.8 γ-units (Sekanina 1999); and companions E, D, G, and B of comet 168P/Hergenrother, whose decelerations were in a range from 9.2 ± 0.3 to 17.1 ± 2.3 γ-units, although all four belonged to the class of companions of high brittleness (the endurance ranging from 22 to 37 e-days; Sekanina 2010). See also Boehnhardt (2004).

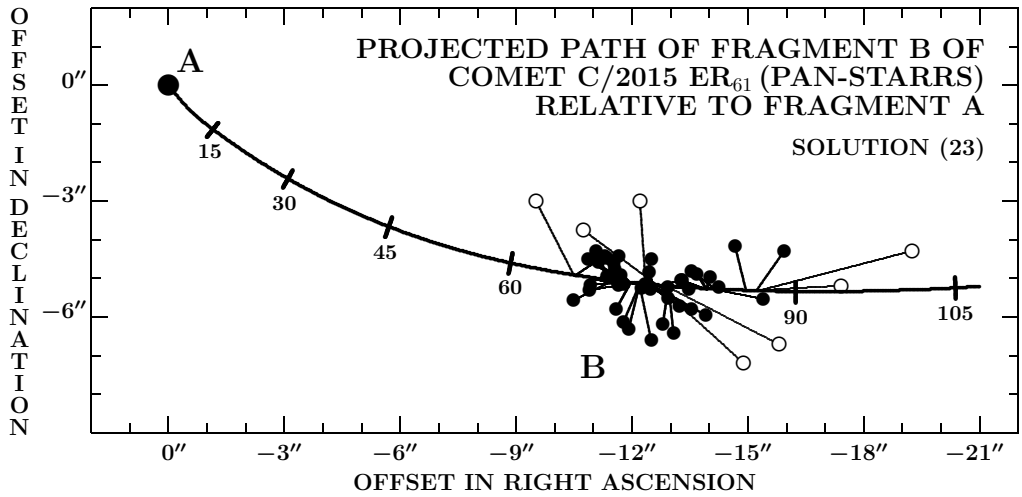


Figure 8. Path of the companion (fragment B) of C/2015 ER_{61} relative to the primary nucleus (fragment A) in projection onto the plane of the sky, as provided by the solution (23) in the equatorial system of coordinates. The solid circles are the B – A offsets that were incorporated into the solution, the open circles are those excluded because they left residuals exceeding ±1″.5 in one or both coordinates. The numbers along the path are days from fragmentation on 2017 April 5.2 UT (60 days refers to June 4.2 UT, 90 days to July 4.2 UT, etc.).

and endurance of the companion. The parameters and other data describing this final solution are:

$$\begin{aligned}
t_{\rm frg} &= 2017\ \text{April 5.2 UT},\\
t_{\rm frg} - t_\pi &= -34.7\ \text{days},\\
\gamma &= 14.3\ \gamma\text{-units},\\
V_{\rm sep} &= 0.90\ \text{m s}^{-1},\\
V_{\rm R} &= +0.38\ \text{m s}^{-1},\\
V_{\rm T} &= -0.69\ \text{m s}^{-1},\\
V_{\rm N} &= -0.44\ \text{m s}^{-1},\\
E &= 69\ \text{e-days},\\
\text{Mean } O\text{–}C &= \pm 0''.65,\\
\Sigma\,(O\text{–}C)^2 &= 34.675\ \text{arcsec}^2,\\
\text{Total Dataset} &= 49\ \text{offsets},\\
\text{Dataset Used} &= 42\ \text{offsets},\\
\text{Time Span Covered} &= 2017\ \text{June 11.4–30.4 UT}. \qquad (23)
\end{aligned}$$

To complete the portrayal of the companion's birth and orbital evolution in terms of the solution (23), I plot in Figure 8 its resulting path relative to the primary nucleus and list in Table 7 the 49 offsets and their "observed minus computed," or *O–C*, residuals from the solution. Each offset entry in this table is a difference between a single astrometric position of the companion and an average of up to 12 motion-corrected astrometric positions of the primary nucleus at times of up to 0.01 day apart. An internal error of these averaged offsets is typically ±0″.4 in right ascension and ±0″.3 in declination. Seven of the 49 tabulated offsets were excluded from the solution because they left residuals (parenthesized in Table 7) in excess of ±1″.5 in one or both coordinates. The table shows that the distribution of residuals of the included offsets is satisfactory in that it exhibits no systematic trends in either right ascension or declination.

As a final comment on the companion's relative motion, I should mention that Bachini (2017), of Stazione Astronomica BS-CR, Santa Maria a Monte, Italy, observing with a 25-cm f/10 Schmidt-Cassegrain with an f/6.3 focal reducer (Code K47), is reported as having provided a set of four astrometric observations of the companion, spanning 17 minutes on 2017 August 23.[14] Four circumstances that make this identification highly suspect include: (i) a nuclear magnitude of 14.6, which is comparable to the brightness of the primary nucleus reported at the time by other observers; (ii) a gap of nearly 8 weeks from the previous observation of the companion; (iii) no simultaneous astrometry of the primary; and (iv) the orbital elements for the companion from a solution that incorporated these dubious astrometric positions (*Minor Planet Center* 2017) being listed with no mean residual of the fit, which is extremely unusual. Because of (iii), one cannot compute the B – A offset, but the residuals from the orbit of the primary are a fair proxy for the missing offset. They average +21″ in right ascension and +3″ in declination. The solution (23) predicts for August 23 the companion's offset of −32″ in right ascension and −5″ in declination, leaving enormous residuals of +53″ and +8″ in the two coordinates, respectively. When the August 23 proxy offset was incorporated into the input dataset, the resulting solution failed miserably, leaving strong systematic residuals of several arcsec. There is no doubt whatsoever that the August 23 astrometric positions reported from Code K47 refer to the primary nucleus, but are off, especially in right ascension. As a result, the published parabolic orbital elements for the companion from a solution that incorporated these positions (*Minor Planet Center* 2017) are meaningless.

5.7. *Companion's Light Curve*

If the comet's nucleus split in the course of the outburst, then the question of why it took more than nine weeks to detect the companion for the first time needs to be answered. While cometary companions are never recognized by a terrestrial observer soon after the breakup

[14] Because of the brevity of recorded astrometric observations in the *Minor Planet Circulars*, one cannot rule out a possibility that the positions were attributed to the companion (rather than to the primary) by the *Minor Planet Center*'s staff, not by the observer.

because of their proximity to the primary, the proposed solution (23) suggests that the separation between the fragments was 2″ on April 22, 17.6 days after breakup; 4″ on May 5, 30.3 days after breakup; and 6″ on May 16, 41 days after breakup. Thus, insufficient separation distance is unlikely to provide an explanation for the considerable delay, and the apparent culprit may instead be the companion's excessive faintness. In a search for evidence of the suspected cause, I compiled and normalized the companion's CCD nuclear magnitudes and compared the resulting light curve with that of the primary nucleus obtained from the same data sources. The results turned out to be quite compelling.

The data points, plotted in Figure 9, are averages from the nuclear magnitudes reported by the six sources listed in Table 5 and by the observers at Stixendorf, Austria (code A71; see the caption). The individual magnitudes were measured by the observers in images taken in rapid succession covering periods of up to ∼20 minutes (for the reference, see footnote 2). Each average has an internal mean error that measures a combined effect of observational uncertainties and genuine brightness fluctuations on a scale of a fraction of one hour. The figure depicts dramatic differences between the photometric behavior of the primary and the companion on several time scales:

Table 7
Offsets of Companion B Relative to Primary Nucleus A of C/2015 ER_{61} Derived from Astrometric Positions, and Their Residuals from Solution (23)

Time of Observation 2017 (UT)	Offset of B from A		Residual $(O-C)$[a]		Obs. Code
	in R.A.	in Decl.	in R.A.	in Decl.	
June 11.41312	−9″.52	−3″.00	(+0″.99)	(+1″.97)	G39
11.41476	−11.30	−4.42	−0.79	+0.55	G39
13.41128	−11.65	−5.17	−0.66	−0.14	G39
13.41483	−11.71	−4.91	−0.72	+0.12	G39
15.41804	−11.66	−4.42	−0.20	+0.67	G39
15.42232	−10.49	−5.57	+0.97	−0.48	G39
16.20876	−11.13	−4.58	+0.53	+0.53	G40
16.21215	−11.36	−4.48	+0.30	+0.63	G40
16.40279	−11.36	−4.94	+0.35	+0.18	G39
16.40611	−10.86	−4.50	+0.85	+0.62	G39
16.41035	−12.93	−5.23	−1.22	−0.11	G39
16.41258	−10.93	−5.17	+0.78	−0.05	G39
17.40299	−11.53	−4.60	+0.42	+0.54	G39
17.40674	−11.07	−4.30	+0.88	+0.84	G39
17.41148	−11.55	−4.77	+0.40	+0.37	G39
17.44641	−11.59	−5.00	+0.37	−0.66	926
17.45247	−10.90	−5.31	+1.06	−0.17	926
17.46001	−11.79	−5.14	+0.17	0.00	926
18.40296	−12.50	−6.60	−0.30	−1.43	G39
18.40551	−11.92	−6.30	+0.27	−1.13	G39
18.40913	−11.78	−6.14	+0.42	−0.97	G39
18.41219	−11.42	−5.00	+0.78	+0.17	G39
19.06274	−12.21	−3.00	(+0.14)	(+2.18)	C10
19.07575	−12.50	−4.50	−0.14	+0.68	C10
19.40372	−13.23	−5.73	−0.79	−0.54	G39
19.41115	−12.94	−5.51	−0.50	−0.32	G39
19.41338	−12.48	−5.28	−0.04	−0.09	G39
19.80124	−13.47	−5.27	−0.93	−0.07	Q62
19.80299	−13.54	−5.79	−1.00	−0.59	Q62
19.80647	−12.45	−4.83	+0.09	+0.37	Q62
19.81422	−13.91	−5.95	−1.37	−0.75	Q62
20.20874	−12.24	−5.25	+0.40	−0.05	G40
20.21234	−13.30	−5.05	−0.66	+0.15	G40
20.40378	−14.89	−7.19	(−2.20)	(−1.98)	G39
20.41275	−10.75	−3.76	(+1.94)	(+1.45)	G39
21.43911	−15.81	−6.71	(−2.86)	(−1.48)	926
21.44062	−12.80	−6.19	+0.15	−0.96	926
21.44231	−13.08	−6.41	−0.14	−1.18	926
23.41710	−14.25	−5.15	−0.81	+0.11	W96
23.42492	−12.34	−5.25	+1.10	+0.01	W96
25.40441	−13.68	−4.88	+0.26	+0.41	G39
25.40817	−13.27	−5.04	+0.68	+0.25	G39
25.41330	−14.02	−4.96	−0.08	+0.33	G39
26.40840	−15.39	−5.53	−1.19	−0.23	G39
26.40968	−13.54	−4.81	+0.66	+0.49	G39
29.40836	−14.67	−4.16	+0.30	+1.17	G39
29.41044	−17.41	−5.19	(−2.44)	(+0.14)	G39
30.40892	−19.25	−6.07	(−4.02)	(−0.74)	G39
30.41331	−15.86	−4.29	−0.63	+1.04	G39

Note.
[a] Rejected observations are parenthesized.

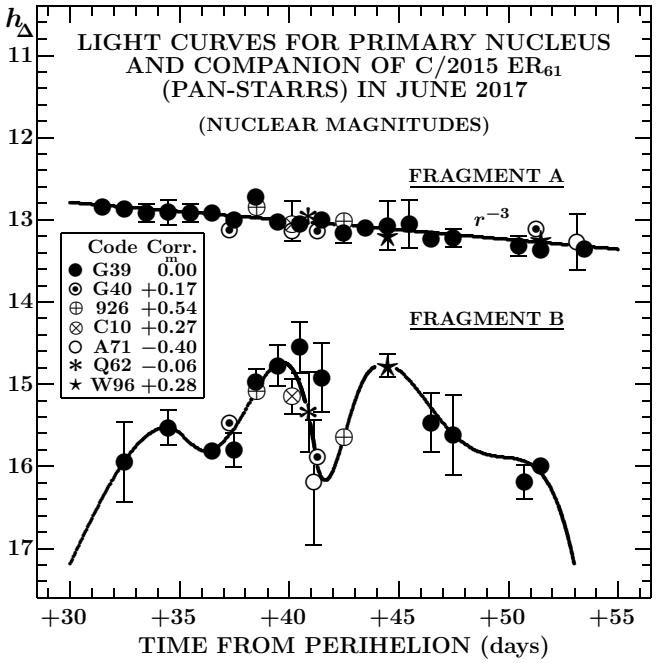


Figure 9. Light curves of the companion (fragment B; bottom) and the primary nucleus (fragment A; top) of comet C/2015 ER_{61} over the entire period of time in June 2017 when the companion was under observation. The plotted CCD nuclear magnitudes h_Δ have been normalized to a unit geocentric distance by an inverse square power law. Although no phase correction was applied, the model by Marcus (2007), based on a compound Henyey-Greenstein dust scattering law, shows that introducing the correction would result in relative changes not exceeding ±0.02 mag (merely shifting the plot up by almost 1 mag) because of a limited range of phase angles. The plot is based on 167 individual nuclear-magnitude determinations for the primary nucleus and 52 such determinations for the companion. They were measured from images taken in rapid succession over less than ∼20 minutes and averaged into 31 and 20 plotted data points for, respectively, the primary nucleus and the companion, with the mean short-term scatter depicted by the error bars. The entries without an error bar have a mean error not exceeding ±0.1 mag, the size of the used symbols. The magnitudes were provided along with astrometric positions by the six sources listed in Table 5 plus by code A71 (Stixendorf, Austria, 30-cm f/4 reflector, observers M. Jäger et al.); the data are available from the *Minor Planet Center*'s database. The fairly smooth light curve of the primary nucleus was used to compute systematic corrections for the observing codes to convert the magnitudes of both fragments to the brightness scale of code G39; the corrections are in the inset.

(1) On a scale comparable to the span of time covered in Figure 9, of approximately three weeks; the primary nucleus was fading fairly smoothly at a rate that closely followed an inverse cube power law of heliocentric distance, whereas the companion was brightening at the beginning but fading at the end at a rapid rate, suggesting that its excessive faintness prior to June 11 was indeed the reason for its nondetection.

(2) On a scale of several days, the brightness variations of the primary nucleus were confined to a rate of seldom higher than 0.1 mag, whereas the amplitude of the companion's brightness fluctuations clearly exceeded 1 mag. The curve fitted to these data points is only a crude approximation to the irregular brightness variations.

(3) The primary nucleus is seen in Figure 9 to have been imaged and measured on many more days than the companion; a possible reason for this disparity could be an intermittent excessive faintness of the companion on the days from which its astrometry is unavailable, providing further potential evidence for its brightness fluctuations on a scale of days.

(4) Although one can expect instrumental errors in determining a magnitude to increase somewhat with decreasing brightness, the difference between the large error bars of the magnitude measurements of the companion compared to the primary nucleus is too striking to be explained by observational uncertainties. The highly unequal error bars imply that the primary nucleus and the companion differed significantly in terms of their brightness fluctuations on a scale of a fraction of one hour.

In summary, I find that a major disparity in the behavior of the two nuclear fragments and a considerably larger amplitude of the companion's brightness fluctuations took place over intervals of time that spanned at least three orders of magnitude. The extreme variability of the companion's activity appears to have been associated with the object's progressive fragmentation that probably resulted in its complete disintegration by the end of June or in the first days of July. Paradoxically, it was this crumbling process that made it possible to detect the companion in the first place; before these developments came about in earnest, we had been unaware of the companion's existence.

Highly irregular variations in the brightness of companion nuclei were repeatedly documented in numerous past investigations of the split comets; the light curves exhibited by fragments of the long-period comets C/1947 X1, C/1956 F1, and C/1975 V1, see Sekanina (1982); of 73P, an example of the short-period comets, see Boehnhardt (2004), Sekanina (2008a).

6. CONCLUSIONS

Two striking phenomena displayed by C/2015 ER_{61}, a dust-poor comet, were an outburst that peaked nearly five weeks before perihelion and a double nucleus that was first noticed about one month after perihelion and was followed for nearly three weeks. Three major objectives addressed in this paper are: (1) the onset and physical evolution of the outburst; (2) the conditions at birth of the companion nucleus B and its orbital and physical evolution in comparison with the primary nucleus A; and, most importantly, (3) a potential close relationship between the outburst and nuclear splitting, in spite of a gap of more than nine weeks between them.

The outburst is detected in, and its timing constrained by, five datasets: (i) a visual light curve; (ii) a light curve based on selected CCD total magnitudes; (iii) a light curve based on selected CCD nuclear magnitudes; (iv) a large-scale imaging; and (v) a curve of the $Af\rho$ parameter, which is a proxy of the comet's dust-production rate. Four of these sets — (i) and (iii) through (v) — turn out to be broadly consistent with the model adopted in this paper: an onset of the outburst 36.0 days before perihelion, on 2017 April 3.9 UT, and a sharp, spike-like peak (typical for dust-poor comets) some 2.6 days later. The visual light-curve data are distributed densely enough that the uncertainty of the onset time can be estimated at as little as ± 0.1 day and the time of peak brightness at ± 1 day. The light curve based on the selected CCD total magnitudes implies instead March 28.6 UT for the onset time, with an estimated uncertainty of ± 1 day. The two critical CCD observations that appear to rule out a later onset time are by T. Takahashi on March 30.8 UT and by H. Abe on April 1.8 UT (Figure 1), both showing the comet's brightness to have become increasingly elevated compared to the level before March 20. The other datasets do not suggest any such effect; the reason for this discrepancy remains unclear.

The rise time, defined as a temporal distance from the onset to the peak brightness, measures the active phase of the outburst. Comparison of C/2015 ER_{61} with some other flaring-up comets suggests that the active phase is usually brief, not exceeding a few days, although there are exceptions, as illustrated by comet 73P in 1995 or by Event III of C/2001 A2 (Table 4). The active phase of 2.6 ± 1 days for the adopted outburst model of C/2015 ER_{61} thus appears to be of a rather typical duration.

Investigated in relation to the primary nucleus A, the motion of the companion B is based on 42 out of a total of 49 B – A offsets in right ascension and declination, which are fitted by a multiparameter model for the split comets (Sekanina 1978, 1982), extensively applied in the past. Some of the solutions obtained for C/2015 ER_{61}, presented in Table 6, suggest that the companion's motion was subjected to a moderate nongravitational deceleration and that the time of the companion's separation from the parent nucleus is rather poorly determined (and highly correlated with the radial component of the separation velocity), but is most probably between 50 ± 8 and 27 ± 9 days before perihelion, or, nominally, between April 21 and May 13, thus bracketing the outburst whose active phase is centered on 34.7 ± 0.5 days before perihelion, or, nominally, on April 5.2 UT. With the high probability that the outburst was a product and signature of nuclear fragmentation, a three-parameter model from Table 6 was further refined by incorporating a relationship between the companion's longevity, or endurance, and nongravitational deceleration for cometary fragments of medium brittleness (Sekanina 1982).[15]

[15] More recently, Boehnhardt (2004) suggested an alternative, averaged fit to an expanded dataset; disregarding the previously introduced classes of fragment brittleness, he finds a much steeper dependence of the endurance on the nongravitational deceleration, even though his plot still shows that the variations among both the most and the least enduring fragments follow a law that is substantially flatter. Application of Boehnhardt's relationship between the endurance and deceleration to C/2015 ER_{61} would result in a solution for the companion that is outside a range judged as plausible by other applied constraints (Section 5.6).

The adopted fragmentation model — solution (23) — indicates that the companion separated from the parent nucleus with a velocity of 0.9 m s^{-1} in a direction generally away from the Sun, opposite to the comet's orbital motion, and below the orbital plane. The deceleration, 14.3 units of 10^{-5} the Sun's gravitational acceleration, offers a crude estimate of less than one hundred meters for the overall dimensions of the companion, too small to detect unless in a state of advanced fragmentation.

This implication appears to be corroborated by observational evidence. Contrary to the primary nucleus, the companion displayed major fluctuations in brightness on time scales that spanned at least three orders of magnitude, from a fraction of one hour to weeks. The more-than-nine-week gap between the companion's birth and its first detection appears to be a corollary of this brightness variability. Specifically, the companion may have been too faint for detection before June 11, a distinct possibility supported by a rapid brightening at the time (Figure 9). Indeed, it apparently was the debris the companion was shedding and activity derived from newly exposed areas of volatile substances — products of progressive fragmentation — that greatly facilitated the detection. Ironically, this same process resulted in the companion's impending disintegration by the end of June or in early July, also in line with the light curve.

The story of an outburst and ensuing nuclear duplicity of comet C/2015 ER_{61} appears to be rather reminiscent of similar phenomena observed in other flaring-up and split comets. In-depth comparison of this object's outburst with such events in a number of past comets was employed to introduce a new set of outburst parameters, while the data on the companion were exploited to offer a comprehensive model for its orbital motion and to investigate an interaction between the companion's orbital and physical properties. The author hopes that, jointly with his recent work on comet 168P/Hergenrother, this investigation contributes both to gaining greater insight into the behavior of the split comets and to the understanding of the physical relationship between outbursts and nuclear fragmentation.

This research was carried out at the Jet Propulsion Laboratory, California Institute of Technology, under contract with the National Aeronautics and Space Administration.

REFERENCES

A'Hearn, M. F., Millis, R. L., Schleicher, D. G, et al. 1995, Icarus, 118, 223
Bachini, M. 2017, MPC 105599
Bessell, M. S. 1979, PASP, 91, 589
Beyer, M. 1962, Astron. Nachr., 286, 219
Bobrovnikoff, N. T. 1927, ApJ, 66, 439
Bobrovnikoff, N. T. 1928, PASP, 40, 164
Boehnhardt, H. 2004, in Comets II, ed. M. C. Festou, H. U. Keller, & H. A. Weaver (Tucson, AZ: University of Arizona), 301
Gibson, B., Goggia, T., Primak, N., et al. 2015, MPEC 2015-F124
Gibson, B., Goggia, T., Primak, N., et al. 2016, MPC 97628
Green, D. W. E. 2016, CBET 4249
Green, D. W. E. 2017a, CBET 4383
Green, D. W. E. 2017b, CBET 4409
Hambsch, F.-J., & Bryssinck, E. 2017, MPEC 2017-N28
Hambsch, F.-J., Bryssinck, E., & Hambsch, J. 2017a, MPEC 2017-M09
Hambsch, F.-J., Bryssinck, E., & Hambsch, J. 2017b, MPEC 2017-N58
Hosek, M. W. Jr., Blaauw, R. C., Cooke, W. J., et al. 2013, AJ, 145, 122
King, B. 2017, `http://www.skyandtelescope.com/astronomy-news/comet-er61-panstarrs-in-outburst-binocular-bright`
Marcus, J. N. 2007, ICQ, 29, 39
Masi, G., & Schwartz, M. 2017, MPEC 2017-M09
Miles, R., Faillace, G. A., Mottola, S., et al. 2016, Icarus, 272, 327
Minor Planet Center 2015, MPEC 2015-F124
Minor Planet Center 2017, MPC 106344
Müller, G. 1884a, Astron. Nachr., 107, 381
Müller, G. 1884b, Astron. Nachr., 108, 161
Nakano, S. 2017, Nakano Note 3379
Primak, N., Schultz, A., Watters, S., et al. 2016, MPEC 2016-C01
Roemer, E. 1959, PASP, 71, 546
Sekanina, Z. 1978, Icarus, 33, 173
Sekanina, Z. 1982, in Comets, ed. L. L. Wilkening (Tucson, AZ: University of Arizona), 251
Sekanina, Z. 1999, A&A, 342, 285
Sekanina, Z. 2000, IAUC 7471
Sekanina, Z. 2005a, Int. Comet Quart., 27, 225
Sekanina, Z. 2005b, IAUC 8562
Sekanina, Z. 2008a, Int. Comet Quart., 30, 3
Sekanina, Z. 2008b, Int. Comet Quart., 30, 63
Sekanina, Z. 2009, Int. Comet Quart., 31, 5
Sekanina, Z. 2010, Int. Comet Quart., 32, 45
Sekanina, Z. 2012, *Giant Explosions, Cascading Fragmentation, and Episodic Aging of Comets*. Academy of Sciences of the Czech Republic, Praha, 184 pp. (In Czech.)
Sekanina, Z., & Kracht, R. 2016, ApJ, 823, 2
Sekanina, Z., Jehin, E., Boehnhardt, H., et al. 2002, ApJ, 572, 679
Trigo-Rodríguez, J. M., García-Hernández, D. A., Sánchez, A., et al. 2010, MNRAS, 409, 1682
Vogel, H. C. 1884, Astron. Nachr., 131, 373